



An integrated model for aquaculture production, pathogen interaction, and environmental effects

Joao G. Ferreira^{a,b,*}, Nick G.H. Taylor^c, Alhambra Cubillo^a, Joao Lencart-Silva^a, Roberto Pastres^d, Øivind Bergh^e, James Guildler^c

^a Longline Environment Ltd, 63, St. Mary Axe, London W1G 8TB, United Kingdom

^b DCEA, Faculdade de Ciências e Tecnologia, Universidade Nova de Lisboa (NOVA), Quinta da Torre, 2829-516 Monte de Caparica, Portugal

^c Centre for Environment, Fisheries and Aquaculture Science, Weymouth, United Kingdom

^d Ca' Foscari University of Venice, via Torino 155, 30172 Mestre, Italy

^e Institute of Marine Research, PO Box 1870, Nordnes 5817, Bergen, Norway

ARTICLE INFO

Keywords:

Carrying capacity
Husbandry
Environment
Production
Pathogen
ABC model
Fish
Shellfish
Salmon
Oyster
IHNv
Herpes
Vibrio
Disease
Climate change

ABSTRACT

This work develops, applies, and tests a methodology for simulating three key determinants of aquaculture carrying capacity: production, environmental effects, and pathogen interactions. Deterministic models for simulation of biomass production and environmental effects for fish and shellfish were combined with stochastic host-pathogen models based on the *Susceptible-Exposed-Infected-Recovered* (SEIR) paradigm to build the Aquaculture, Biosecurity, and Carrying Capacity (ABC) platform. Individual growth models for the finfish species Atlantic salmon (*Salmo salar*) and gilthead bream (*Sparus aurata*), and the bivalve species Pacific oyster (*Crassostrea gigas*) and Eastern oyster (*C. virginica*) were integrated into an Individual Based Model (IBM) capable of scaling to any farm size; the resulting framework was coupled to host-pathogen models for: (i) salmon-Infectious Hepatopoietic Necrosis virus (IHNv); (ii) Pacific oyster-Oyster herpes virus (OsHV-1); and (iii) Pacific oyster-*Vibrio aestuarianus*.

ABC was run for a set of scenarios both with and without pathogens, and results presented for (a) husbandry: food depletion in Eastern oyster, showing the effects of overstocking on production and water-column chlorophyll; an increase in the spacing of farm sections increases yield by 80%; (b) environmental effects: changes due to marine cage culture of gilthead sea bream, and the effect of hydrodynamics on reduction of dissolved oxygen (DO) and increase in ammonia; a farm sited in a high-dispersion area shows a variation of about 1.5 mg L⁻¹ in DO among cages, whereas the range in a low-dispersion site can be up to 5 mg L⁻¹; (c) three case-studies of pathogen interaction: (i) effects of a salmon-IHNv pathogen event on yield and mortality, and consequences of event timing (early- or late-stage in the culture); the late-stage event costs almost 300,000 USD more in wasted feed, and the Feed Conversion Ratio (FCR) increases from 1.5 to 2.3; (ii) consequences for a *Vibrio* outbreak in oysters; even though the disease event is very short, there is a 7.8% decrease in oyster harvest, and net nitrogen removal, a key regulatory ecosystem service, decreases by 10.2%; and (iii) climate change scenarios based on Representative Concentration Pathway (RCP) 8.5 and consequences for a herpes outbreak in oysters; ABC results show that the *direct* effect of climate change on growth, which leads to earlier harvest and less non-harvestable animals, is strongly outweighed by the *indirect* effect of a pathogen outbreak, which results in a 27.8% increase in dead biomass and a 28.6 t (20.1%) reduction in harvested biomass. Furthermore, since there is a relationship between the colonisation of *C. gigas* by *Vibrio* and full-blown outbreaks of oyster herpes, climate change may lead to synergistic mortality effects of significant concern to oyster growers in temperate waters.

The importance of a combined approach to aquaculture carrying capacity that includes the disease component and its relationship to environmental stressors is discussed, together with the management relevance and potential application by industry of an integrated framework.

* Corresponding author at: Longline Environment Ltd, 63, St. Mary Axe, London W1G 8TB, United Kingdom.

E-mail address: joao@hoomi.com (J.G. Ferreira).

<https://doi.org/10.1016/j.aquaculture.2021.736438>

Received 23 July 2020; Received in revised form 22 January 2021; Accepted 24 January 2021

Available online 30 January 2021

0044-8486/© 2021 Elsevier B.V. All rights reserved.

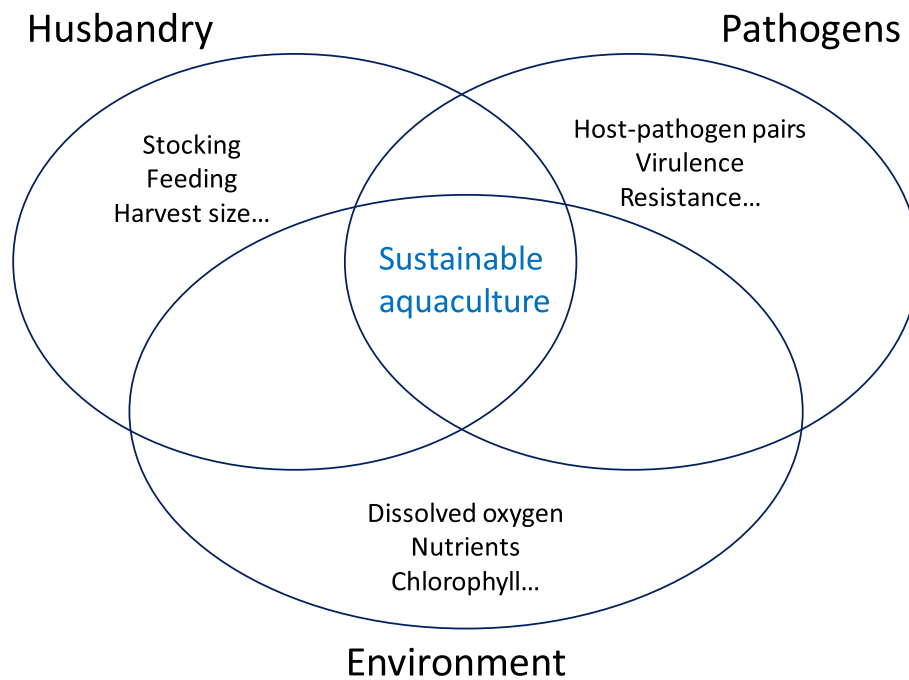


Fig. 1. - Framework for carrying capacity assessment. The husbandry, environment, and pathogen categories together determine the sustainability of the activity. A list of the more relevant indicators in each category is included.

1. Introduction

In May 2013, aquaculture overtook capture fisheries as the primary source of aquatic products for direct human consumption (FAO, 2020), a paradigm shift equivalent to the change from hunting and gathering to agriculture during the Neolithic period, 400 generations ago. In view of an increasing global population and the global decline in wild fish catch, this appears to be an irreversible trend.

The European Union now imports 68% of the aquatic products it consumes (European Commission, 2018), and the United States imports 86% (Tiller et al., 2013). Some of these fish and shellfish are supplied by their northern neighbours: Norway currently cultivates $1.4 \times 10^6 \text{ t y}^{-1}$ of Atlantic salmon (*Salmo salar*) and rainbow trout (*Oncorhynchus mykiss*), more than the entire EU aquaculture production for all species (Eurostat, 2019), and Canada produces $1.91 \times 10^5 \text{ t y}^{-1}$ (Fisheries and Oceans Canada, 2020) of which 60% is Atlantic salmon (Ferreira and Bricker, 2019).

At present, 90% of aquaculture produce on the planet comes from SE Asia and China, which are major exporters, but in India and China alone, consumption of these products has increased by 20 million tonnes in under a decade (FAO, 2008; FAO, 2014). Growth of internal market demand is expected to result in a further increase of 14 million tonnes by 2025 (FAO, 2016; Lopes et al., 2017). This is partly explained by population growth, but the other major factor is a significant increase in per capita GDP (JCER, 2018).

Taken together with an estimated world population of almost 10 billion by 2050 (Cressey, 2009), this presents a huge food security challenge for both the European Union and United States. A substantial effort is therefore being placed on the sustainable development of aquaculture in these regions. However, this expansion is hindered by overregulation (Váradi et al., 2011) and lack of social licence (Shafer et al., 2010; Murray and D'Anna, 2015), and also by a lack of tools to help analyse the ecological effects of this development at a number of levels: these risks include introgression for wild populations due to escape of cultivated fish (e.g. Atalah and Sanchez-Jerez, 2020), and pathogen-related issues for both farmed and wild animals (Alaliyat et al., 2019; Flores-Kossacka et al., 2020).

Over the last two decades, a substantial research effort has been

placed on modelling of individual growth of different aquatic species, with a particular emphasis on those that are cultivated commercially such as Atlantic salmon (Stigebrandt et al., 2004; Føre et al., 2016), gilthead bream (Hernández et al., 2003; Ferreira et al., 2012a; Nobre et al., 2019), seabass (Stavrakidis-Zachou et al., 2019), tilapia (Ferreira et al., 2014a), shellfish such as mussels (Brigolin et al., 2009) and oysters (Ren and Ross, 2001; Gangnery et al., 2003), and potential candidate organisms (Van der Veer et al., 2006; Cubillo et al., 2016). The main objective of such models is to represent growth in biomass, although some also simulate environmental effects—all these Individual Based Models (IBM) operate within a framework that makes an explicit link with physical and biogeochemical determinants.¹

Several of these models (e.g. Gangnery et al., 2004; Brigolin et al., 2009; Nobre et al., 2010; Nunes et al., 2011; Ferreira et al., 2014b; Filgueira et al., 2014; Cubillo et al., 2016) have been incorporated into broader, population-dynamics simulations, where mortality is typically included as a forcing function, based on reported data from industry sources. While IBMs for major cultivated species are already acceptable in terms of accuracy of predictions, practically none of these deterministic simulations consider the effect of disease (Hoffmann et al., 1995, and Bidegain et al., 2017, are exceptions), and neither has the effect of pathogens been included when these models are scaled to the population level. Farm-scale predictions of yield and environmental effects are thus constrained because disease events, which often have major consequences, are not included. In system-scale models this is also a liability, since hydrodynamic connectivity is frequently a major factor in spatial distribution of pathogens, and consequently a determinant for both site selection and carrying capacity.

The literature that establishes the current definition of carrying capacity for aquaculture (Smaal et al., 1998; Inglis et al., 2000; McKindsey et al., 2006; Ferreira et al., 2013a; Ferreira et al., 2013b) does not refer pathogens, despite the fact that disease is a strong conditioning factor of

¹ Models that use the Gompertz or von Bertalanffy approaches are not considered, since they do not make the necessary connection with environmental drivers of growth and are of limited use in integrated costal management.

ecological carrying capacity, and implicitly included in the FAO definition of the Ecosystem Approach to Aquaculture (EAA, Soto et al., 2008).

In parallel, pathogen impact in cultivated aquatic organisms is often modelled based on the methods described by Kermack and McKendrick (1927) and Anderson et al. (1981), which generally assume a population can be partitioned into a series of coupled states relating to disease status, often: Susceptible-Infected-Recovered (or Removed) (SIR). These models do not follow individuals but track the proportion (or number) of the population in each of these states over time, with transmission of the agent occurring based on the rate at which susceptible and infected hosts interact (which is often density-dependent), or, based on the probability of infection given the infectiveness of the environment (Murray, 2009). Generally, a fixed background mortality is associated with all states, with an additional fixed mortality term being associated with the infected population. If individual growth is included, it is generally in a rudimentary form by means of a growth coefficient, without any representation of physiological processes.

Though pathogen spread between sites can be modelled using similar approaches (e.g. Taylor et al., 2011), network-based models are generally favoured where suitable data is available (e.g. Adams et al., 2012; Jones et al., 2019; Cantrell et al., 2020). These IBMs assume a network of sites/units (nodes) are connected to one another via different pathways (e.g. animal movements and hydrodynamic connections). Unlike the SIR type modelling approach, which assumes that the population mixes randomly with the probability that two individuals contacting each other being equal, network approaches provide a risk-based approach to assigning contacts and transmission risk which can provide a more accurate prediction of disease spread over a geographic range and allow individuals at high risk of getting or spreading a pathogen to be identified. Though known to be important, studies that link within farm processes and disease dynamics with spread through a network are however uncommon (e.g. Salama and Murray, 2011; Salama and Rabe, 2013), and existing studies fail to address aquaculture carrying capacity in a quantitative manner, since they do not typically contain any coupling mechanisms to hydrodynamic, biogeochemical, or physiological models, or combinations thereof.

Animal growth, pathogen interactions, and environmental effects are the three key components of carrying capacity assessment (Ferreira et al., 2013a). An integrated model for these three components (Fig. 1) is presented here for the first time through the development of the Aquaculture, Biosecurity, and Carrying Capacity (ABC) framework.

ABC incorporates stochastic functions for pathogen infection and transmission, both within and among farms, into an IBM farm-scale model that simulates growth deterministically, based on the physiology of the cultivated species.

The objectives of our work were to (a) make a substantial improvement to the state-of-the-art of aquaculture modelling by explicitly accounting for the role of pathogens; (b) analyse the consequences of disease outbreaks on harvestable biomass, environmental sustainability, and economic performance; (c) provide coastal managers with a robust tool for decision support in terms of site selection and carrying capacity, taking into account both intra- and inter-farm effects.

2. Methods

The general framework for the ABC model is presented in Fig. 2; it includes: (i) the physics of the farm area; (ii) husbandry of the cultivated species; (iii) host-pathogen interactions; and (iv) environmental effects of aquaculture.

An outline of the development stages is shown in Fig. 3, as a guide to the sections below.

2.1. Physical framework

ABC considers a bi-directional one-dimensional series of physical

sections (Fig. 2), which may contain cultivated organisms (labelled *Box*). Empty sections (labelled *Gap*) are functionally equivalent to the separation between finfish cages, mussel rafts, oyster trestles, or other structures. ABC transports dissolved and particulate water properties, including pathogens, through bi-directional, tide-dependent advection in the X coordinate, and dispersion in the Y coordinate (Eq. 1):

$$\frac{\partial C}{\partial t} = -u \frac{\partial C}{\partial x} + k_y \frac{\partial^2 C}{\partial y^2} + f(C) \quad (1)$$

Where: C: concentration of any dissolved or particulate water property; t: time (d); x and y: farm section length and width; u: horizontal water velocity normal to farm cross-section (m d⁻¹); k_y: lateral dispersion coefficient (m² d⁻¹); f(C): non-conservative processes. These depend on the state variable simulated and include e.g. physiological processes for simulation of individual growth, and pathogen uptake and decay. These processes are reviewed in the following sections.

The horizontal velocity field is determined from the specification of the typical maximum current speeds at spring and neap tide. A double-sinusoidal function is applied to generate the current speed over the semi-diurnal tidal cycle. Dispersion in the y-coordinate is determined for each section of the one-dimensional system (Fig. 2) by considering lateral boundary conditions where the external concentration of any variable is equal to the upstream boundary in the x-coordinate.

A finite difference scheme is used to solve equations in ABC; the model checks for numerical stability for advective transport by verifying the Courant condition, and for lateral dispersion by verifying the stability criterion shown in Eq. 2 (Press et al., 2002).

$$\frac{2k_y \Delta t}{(\Delta y)^2} \leq 1 \quad (2)$$

Since animals (finfish or shellfish) are cultivated within specific model sections, the advective and dispersive terms of Eq. 1 do not apply to variables such as individual biomass and mortalities but do apply to physiological state variables such as faeces or pseudofaeces.

2.2. Individual modelling

Individual growth models were conceptualised, calibrated, and validated for Atlantic salmon, rainbow trout, gilthead bream (*Sparus aurata*), European seabass (*Dicentrarchus labrax*), Pacific oyster (*Crassostrea gigas*), eastern oyster (*C. virginica*), blue mussel (*Mytilus edulis*), Mediterranean mussel (*M. galloprovincialis*), Manila clam (*V. philippinarum*), and geoduck (*Panopea generosa*).

The individual growth models use a net energy balance (NEB) approach and have been published elsewhere (e.g. Ferreira et al., 2012a; Ferreira et al., 2014a; Saurel et al., 2014; Cubillo et al., 2016; Cubillo et al., 2018), so only key modifications will be described here.

For use in an IBM framework that simulates cultivated animals, each individual in the population is 'created' following the object-oriented paradigm as applied to ecological modelling, originally formulated by Silvert (1993), and Ferreira (1995). The properties of these objects include a number of attributes related to their growth performance, pathogen status, and environmental interactions (e.g. food eaten, particulate organic waste etc). Individuals may die during the culture cycle and therefore mortality status is an intrinsic property of each. The physiological models referred above are all deterministic, but since our objective is to simulate the typical variance of a cultivated population, the individuals that comprise it are stochastically assigned a fitness parameter in terms of assimilation efficiency AE ($\pm 0-5\%$ of the mean AE); this simulates genetic variation within the single cohort of organisms typically deployed at grow-out stage. Fitness is generated at

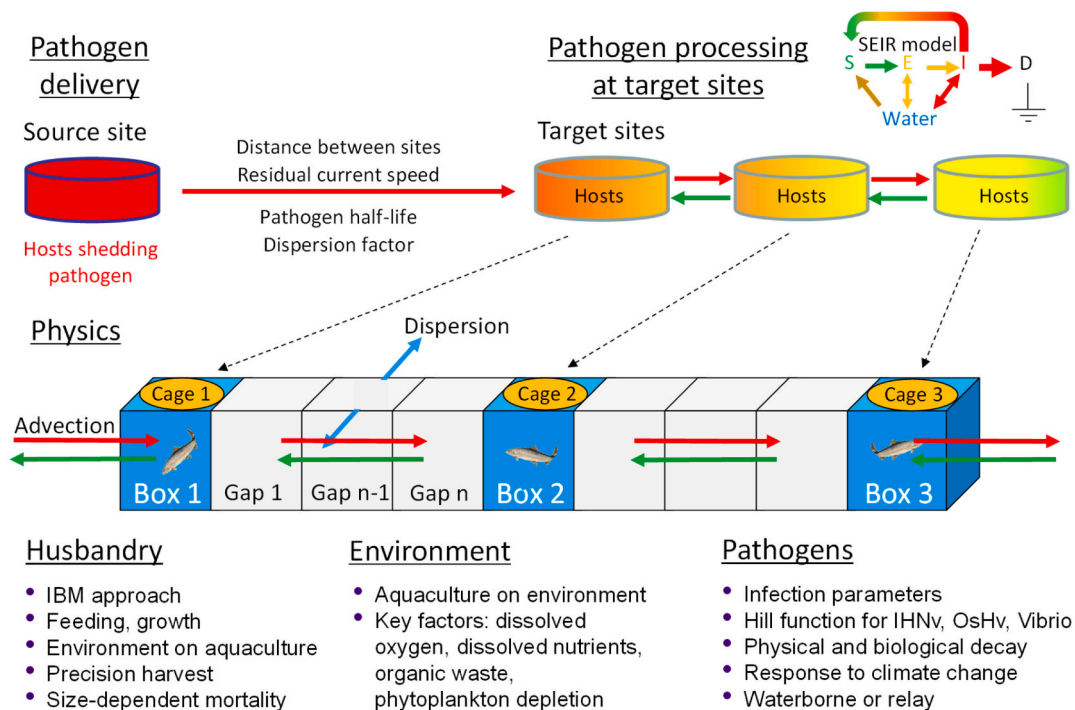


Fig. 2. - General framework for the ABC model. The physical layout of the modelling framework is represented in the upper pane and includes physical processes for exchange of water and water properties (e.g. oxygen, pathogens); the lower pane details key processes and parameters for the three categories that constitute the ABC framework for sustainability.

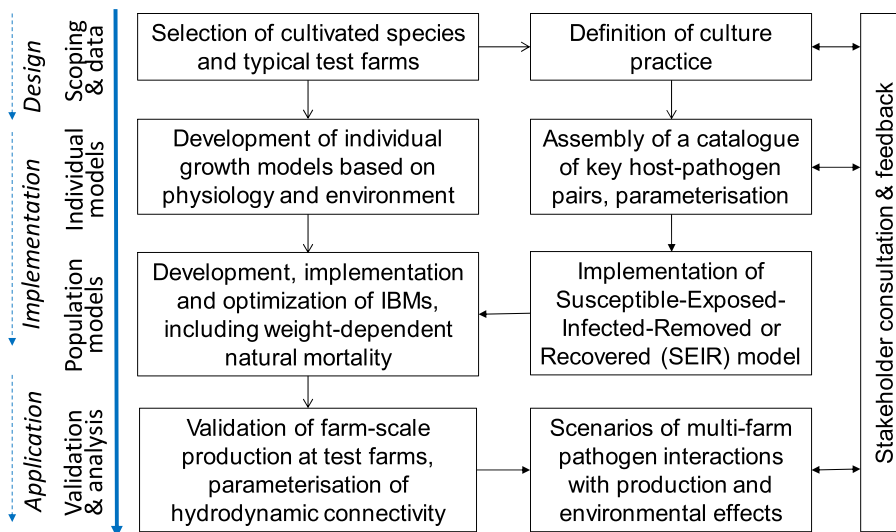


Fig. 3. - Stepwise development of the ABC model. The flowchart represents the key steps required to develop a framework for growth, environment, and pathogen modelling, and includes components such as definition of culture practice and growth validation that make stakeholder consultation and feedback mandatory.

runtime, so the probability of two model runs being identical is extremely small.²

2.3. Population modelling

2.3.1. Estimation of minimum population

The simulation of large populations is not time-efficient, and

² However, ABC can use a constant random number seed to initialise its pseudo-random number generator (PRNG) to produce identical runs.

particularly for bivalves, where millions of organisms may be cultivated in a farm, a minimum sample size for accurate simulation must be determined. This sample size can then be scaled to a greater number of organisms, allowing large populations to be simulated realistically with an acceptable model run time. There is an underlying assumption that the population is normally distributed. This was tested on a population of 10,000 individuals by plotting a frequency distribution of the endpoint live weight for Pacific oysters (Fig. 4).

In ABC, considering a first approach where disease was not simulated, two stochastic functions were used to provide a realistic approximation to a normally distributed population: (i) a random variation of

assimilation efficiency; and (ii) a weight-dependent probability of death which is used to test whether an organism will die at a particular model timestep.

The minimum population was determined using a similar approach to Brigolin et al. (2009), by analysing the variation in the first and second moments of the probability density function. Populations of 100, 200, 500, 1000, 2000, 5000, 10,000, 15,000, and 100,000 individuals were compared, using as metrics the mean day of death and respective variance, and the mean endpoint weight of live animals, and its variance. A further comparison was made of the mean mortality rate and its variance. In all cases, only insignificant differences were observed from 10,000 individuals upwards (Fig. 5).

A further analysis was made of ten replicates of model runs using 10 K and 100 K individuals. Standard statistics were calculated, including mean and standard deviation of endpoint live weight, or day of death (for organisms that died during the model run), as well as percentile 10, 25, 50, 75, and 90 of live weight, and the standard deviation of the median. A two-tailed heteroscedastic *t*-test was applied to the means of the ten replicate data series to test the null hypothesis that no difference existed between observed 10 K and 100 K data series (Table 1).

For both the end-point live weight and the day of death, the *t*-value is well within the confidence interval for $p < 0.001$, which suggests that the means for the two population samples can be considered identical at a 99.9% significance level. On this basis, the ABC model was adapted to consider a population size of 10,000 individuals, which can then be scaled to any greater number.

2.3.2. Natural mortality

Population models typically apply a mortality rate that causes a proportion of individuals to be removed from the population at each calculation time step. Some variation can be imposed e.g. in models that use size classes, such as the Farm Aquaculture Resource Management (FARM) model (Ferreira et al., 2007), by applying different discrete rates depending on organism size; however reported mortality data are often anecdotal, and it is usual to consider an average rate. This occurs in part because mortality in working farms is hard to predict, and the underlying causes, which may range from a hypoxic event to a harmful algal bloom (HAB) or a pathogen outbreak, are poorly understood and impossible to time. Event distribution is mainly stochastic and linked to HABs or pathogens that are not included in growth models. As an example, mortality of eastern oysters in Long Island Sound, USA, may vary between 30 and 80% per year depending on the incidence of *Haplosporidium nelsoni* (Bricker et al., 2018), and MSX outbreaks cannot presently be predicted.

ABC considers both natural and disease mortality. Natural mortality can either be constant or follow a decay function where mortality decreases as a function of weight (Eq. 3):

$$\frac{d\mu_w}{dW} = -\alpha\mu_w \quad (3)$$

where: μ_w : weight-dependent mortality coefficient (d⁻¹); W : individual weight (g DW); α : proportionality constant;

Eq. 3 is integrated analytically to yield:

$$\mu_w = \mu_0 e^{-\alpha W} + m_b \quad (4)$$

where: m_b : integration constant representing the baseline mortality.

The coefficients μ_w , α , and m_b can be user-defined. At each model time step, a randomly-generated probability of death is tested against the mortality coefficient μ_w of each individual, calculated based on its biomass, to determine whether the organism remains in the population. The IBM array stores the day of death of any individual removed.

2.4. Pathogen simulation

The development of the simulation is divided into three parts: (i)

pathogen delivery to the target area; (ii) uptake and effect of the pathogen on the host organism; and (iii) spread throughout the host population, within and among physical sections of the farm.

2.4.1. Pathogen delivery from source

ABC considers waterborne infection through pathogen emission from a source site (e.g. a finfish cage) at a user-defined distance from the nearest structure in farm area (target). Table 2 shows the set of parameters used by ABC for an Atlantic salmon farm contaminated with Infectious Hematopoietic Necrosis virus (IHNV) – a pathogen of international importance listed as notifiable by the Office International des Epizooties (OIE, 2019).

Eqs. 5 to 8 represent the delivery of pathogen from the source site (i.e. the primary emission site) to the farm itself. The processes considered are shown in Fig. 2 (pathogen delivery section) and described by these equations, which deal with loading, travel time to target based on a residual current velocity, pathogen die-off, and pathogen dispersion.

The Load L_s is given in Eq. 5:

$$L_s = A_s I_s S_s \quad (5)$$

Where: A_s : Number of animals at source; I_s : Proportion infected at source; S_s : Shedding rate per individual at source.

Pathogen loading at target (L_t) is lower than L_s due to two types of decay that occur over the transport period (Eq. 6), both of which are related to connectivity, i.e. the distance between source and target and the time of travel.

$$t = \frac{d}{u_r} \quad (6)$$

Where: t : time taken for pathogen to travel from pathogen source to target (d); d : distance between pathogen source and target (m); u_r : residual current velocity (m d⁻¹).

Pathogen die-off depends on the pathogen half-life in the water and on dispersive mixing as the water (containing pathogen particles) is advected from the source site to the target site: both effects dilute the pathogen plume prior to reaching the first target section of the farm.

This may be represented as a first-order decay (Eq. 7):

$$\frac{dP_w}{dt} = -(k_b + k_p)P_w \quad (7)$$

Where: P_w : pathogen concentration in the water³; k_b : pathogen die-off (decay) constant = $\ln(2)/T_{1/2}$ (d⁻¹); k_p : pathogen dilution constant (d⁻¹).

Integrating and multiplying by the advective flow Q (m³d⁻¹) yields (Eq. 8):

$$QP_w = QP_0 e^{-(k_b + k_p)t} \quad (8)$$

Where: $QP_0 = L_s$ and $QP_w = L_t$.

2.4.2. Pathogen processing within the farm

The concentration (C) of the pathogen at the farm site (e.g. within a cage) is obtained through the advective and dispersive exchange shown in Eq. 1, and a standard mass balance equation for $f(C)$, the source and sink terms (Eq. 9):

$$Vf(C) = \tau B_e + \varphi B_i - \sigma B_t \quad (9)$$

³ P_w is used to represent the pathogen concentration at delivery to target (i.e. to the farm). This is a specific case of the generic variable C , which denotes the concentration of any model state variable of the ABC model calculated using Eq. 1.

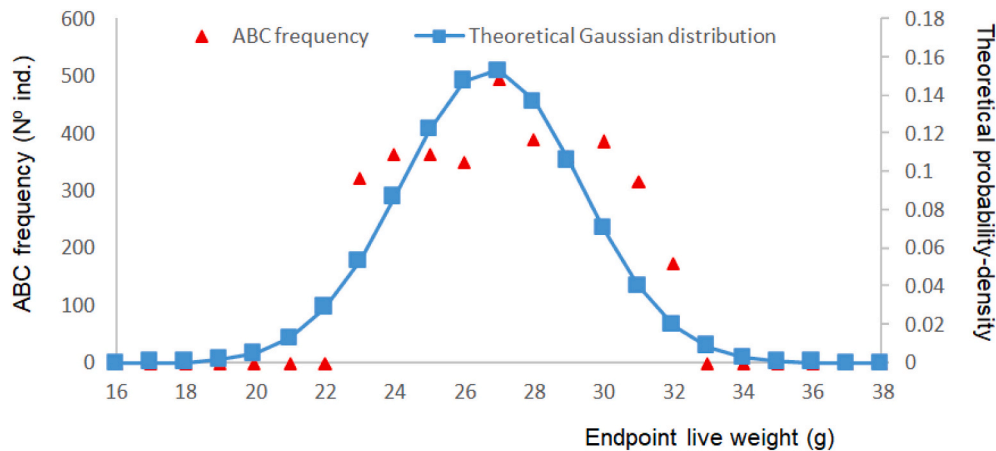


Fig. 4. Frequency distribution of end-point live weight for Pacific oysters from a 10,000 individual model run in ABC, compared to the theoretical Gaussian probability-density function.

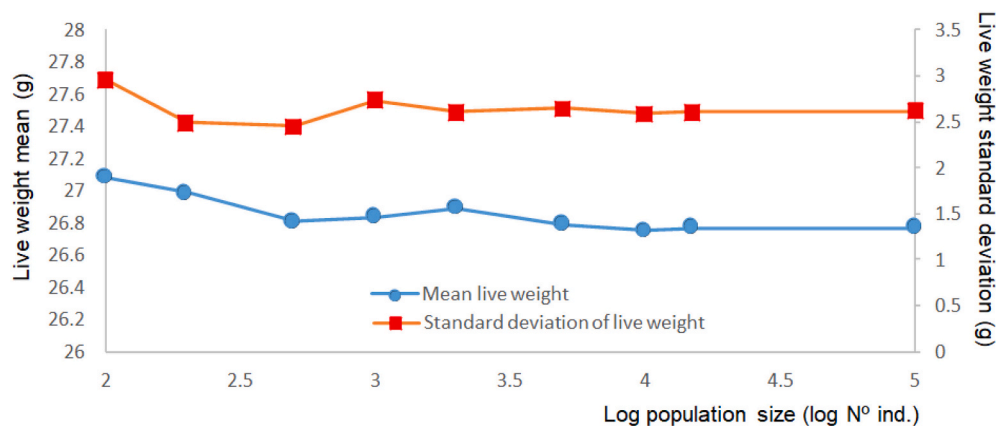


Fig. 5. Variation in first and second moments of probability density function. Upward of 10,000 individuals there is virtually no change (2nd moment expressed as standard deviation rather than variance).

Table 1
t-statistics for average outputs of 10 runs with 10,000 and 100,000 individuals for a $p < 0.001$ level of significance.

Statistic	10 k live weight	100 k live weight	10 k day of death	100 k day of death
Mean	26.75288	26.75852	206.4162	206.0923
Variance	0.000788	7.21E-05	5.398045	0.396006
Observations	10	10	10	10
Hypothesized Mean Difference	0		0	
Degrees of freedom	11		10	
t Stat	-0.60801		0.425591	
P(T ≤ t) two-tail	0.555527		0.67942	
t Critical two-tail	4.436979		4.586894	

Where: V: site (e.g. cage) volume (m³). σ: uptake rate of pathogen (pathogen units⁴ g⁻¹ d⁻¹). B_t: total, i.e. susceptible (S) + exposed (E) + infected (I) biomass of cultivated organisms (g). τ: shedding rate of pathogen for exposed organisms (pathogen units g⁻¹ d⁻¹). B_e: biomass of exposed (E) organisms (g). φ: shedding rate of pathogen for infected organisms (pathogen units g⁻¹ d⁻¹). B_i: biomass of infected (I) organisms (g).

⁴ Units vary depending on the type of pathogen, e.g. for a virus, plaque-forming units, or pfu, will be used.

Table 2
Parameters for the IHN pathogen component of the ABC Atlantic salmon model.

Parameter	Value	Units	Notes
Animals at source (A _s)	50,000	ind.	Calibration
Proportion infected at source (I _s)	5	%	Taylor, pers. com.
Peak shedding rate per individual at source (S _s)	3.2 × 10 ⁷	pfu ind ⁻¹ h ⁻¹	Garver et al., 2013
Pathogen loading at source (L _s = A _s I _s S _s)	1920 × 10 ⁹	pfu d ⁻¹	Normalized time units
Half-life of pathogen decay (T _{1/2})	4.37	d	Garver et al., 2013
Distance to target site	3000	m	Calibration
Duration of pathogen release from source (d)	15	days	Taylor, pers. com.
Residual current speed (v _r)	0.05	m s ⁻¹	Calibration
Dilution factor due to turbulent diffusion (d _p)	0.5	d ⁻¹	Calibration

A precautionary value was chosen, although prevalence can be substantially higher. The assumption is that the farmer would become aware of the issue at higher prevalence and notify the authorities. For the same reason, a relatively short pathogen release period was selected.

Median shedding rate: 3344 pfu g⁻¹ h⁻¹ or 80,267 pfu g⁻¹ d⁻¹ (10⁶ pfu fish⁻¹ h⁻¹ for a 299 g fish) as per Table 3

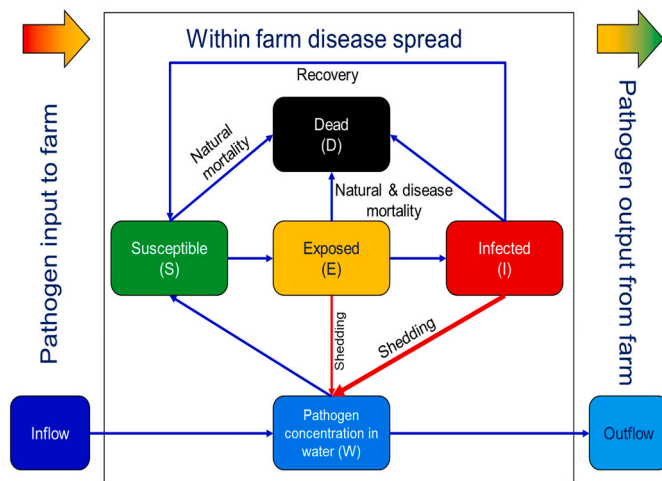


Fig. 6. Schematic representation of the pathogen model in ABC.

Fig. 6 shows the general scheme representing host-pathogen interaction.

Cultivated animals take up the pathogen from the water based on their physiology. Finfish uptake is simulated as a function of ventilation rate, forced by water temperature and allometry, and shellfish uptake is modelled as a function of clearance rate, forced by a complex set of drivers, including chlorophyll (chl), suspended particulate matter (TPM), water temperature, and allometry.

Salmon ventilation rate is calculated following Grøttum and Sigholt (1998), normalized to dissolved oxygen concentration and fish weight, and Pacific oyster clearance rate is determined after Ferreira et al. (2008), with modifications reported in Cubillo et al. (In Press).

In ABC, three internationally important host-pathogen pairings were tested: (i) Atlantic salmon and Infectious Hematopoietic Necrosis virus (IHNV); (ii) Pacific oyster and Oyster herpes virus (OsHV-1); and (iii) Pacific oyster and *Vibrio*. At $t = 0$ all animals are considered to be susceptible to infection and transition from susceptible to exposed based on the quantity of pathogen in the environment, governed by the Hill function (Eq. 10).

$$\beta_p = \frac{P_w^\alpha}{ID50^\alpha + P_w^\alpha} \quad (10)$$

where β_p : probability of infection; α : Hill coefficient of sigmoidicity; ID50: pathogen concentration for 50% infection.

For more opportunistic pathogens such as *Vibrios* (subject to suitable data for parameterisation), it would be straightforward to change the lower limit in order to simulate a higher cut-off threshold for infection, or link the infection curve to particular environmental or stocking conditions, so that infection would only be implemented at times of stress.

Once infected, susceptible (S) organisms enter an exposed (E) state where they show no clinical signs of infection and may only shed pathogen at very low levels. Organisms then transition at rate μ_e into an infectious (I) state where they shed high quantities of pathogen into the environment and remain in this state until they either die from pathogen-induced mortality at rate μ_i (which acts in addition to weight-dependent mortality μ_w - Eq. 3) and are removed from the population, or recover at rate μ_r and stop shedding pathogen—this is therefore an SEIR model, where R represents either removed or recovered. Transitions are calculated using an agent-based approach.

Shedding from infectious hosts determines the pathogen loading to the environment and therefore the rate at which susceptible organisms become infected, but based on hydrodynamic connectivity, this also determines how much pathogen is transported from the site and its subsequent infectiousness to other sites. Data on the coefficients

required for the SEIR model and Eqs. 9 and 10 are scarce, requiring the execution of complex challenge experiments on specific host-pathogen pairs.

The availability of suitable data has therefore in part determined the pathogen pairings used to parameterise the model in this study (presented in Table 3), but the overall framework is highly flexible and can readily be parameterised for most bacterial and viral pathogens given the appropriate data.

Notwithstanding data limitations, the three pairings selected reflect major pathogens that affect key cultivated species, viz. Atlantic salmon and Pacific oyster, and are responsible for significant costs to the industry every year. All three pathogens are waterborne and affect hosts that are usually cultivated in open water (inshore and offshore) systems, and cannot be controlled by vaccination, which makes the development of a predictive management tool all the more relevant.

The pathogen replicates inside the host at an initial rate R_i and, as the host's immune system responds to infection, the pathogen replication rate is reduced to a final rate R_f by means of a first-order decay constant

Table 3

Pathogen model parameters (including Hill function parameters) for the three host-pathogen pairs considered in ABC: IHNV, OsHV-1, and *Vibrio aestuarianus*.

Parameter/species	Atlantic salmon (<i>Salmo salar</i>)	Pacific oyster (<i>Crassostrea gigas</i>)	Pacific oyster
Pathogen	Infectious Hematopoietic Necrosis virus (IHNV)	Oyster herpes virus (OsHV-1)	<i>Vibrio aestuarianus</i>
Hill coefficient of sigmoidicity (α)	1 ^(1,2)	1.7 ⁽⁷⁾	1 ⁽²⁾
Pathogen concentration for 50% infection (ID50)	5.85×10^3 pfu ml ⁻¹ (1)	8.12×10^4 DNA copies ml ⁻¹ (7)	8.4×10^4 (15) - 1.3×10^5 (16) bacteria ml ⁻¹
Uptake rate of pathogen (σ , pathogen units g ⁻¹ d ⁻¹)	Ventilation rate (m ³ g ⁻¹ d ⁻¹)(3) X pfu conc. (pfu m ⁻³)	Clearance rate (m ³ g ⁻¹ d ⁻¹)(8) X DNA conc. (copies m ⁻³)	Clearance rate (m ³ g ⁻¹ d ⁻¹)(8) X bact. Conc. (bact. m ⁻³)
Median shedding rate of pathogen for infected organisms (ϕ)	80,267 (pfu g ⁻¹ d ⁻¹) (4)	1.04 x10 ⁵ (DNA copies g ⁻¹ min ⁻¹)(9)	2.439 x10 ⁷ (bacteria g DW oyster ⁻¹ d ⁻¹) (15)
Shedding rate of pathogen for exposed organisms (τ)	0.1 X ϕ (5)	0.1 X ϕ (5)	0.1 X ϕ (5)
Infected host mortality	0.030 (T _{1/2} = 23 days)(4)	0.173 (T _{1/2} = 4 days) (7,9,10,11,12)	0.099 (T _{1/2} = 7 days) (16)
Optimum temperature range (°C)	8–15(6)	16–24(13,14)	19–30(15)

McKenney et al., 2016, determined from a challenge experiment with duration of 1 h.

²Taylor, pers. com.

³Determined from oxygen uptake rate for each individual at time t and dissolved oxygen in the water at time t.

⁴Garver et al., 2013.

⁵Model calibration.

⁶Bootland and Leong, 1999.

⁷Petton et al., 2015a;

⁸Ferreira and Bricker 2019;

⁹Paul-Pont et al., 2015;

¹⁰Evans et al., 2015;

¹¹Schikorski et al., 2011a;

¹²Schikorski et al., 2011b;

¹³Pernet et al., 2015;

¹⁴Kamermans, pers. com.

¹⁵Lupo et al., 2019; converted from 34,150 bacteria ml⁻¹ oyster⁻¹ d⁻¹ (Lupo, pers. com.; tissue dry weight of a 12 g oyster from Ferreira and Bricker, 2019);

¹⁶Travers et al., 2017.

k_r , where $k_r = \ln(R_f/R_i)/t_p$, where t_p is the duration of pathogen emission from the source. R_f and R_0 are set through model calibration and are host-pathogen specific.

Finally, a host-pathogen-specific baseline immunity coefficient k_i was parameterised to allow the body burden of pathogen in a host to decrease over the long-term during culture cycle.

3. Results and discussion

Results are presented and discussed for the three components of carrying capacity assessment (Fig. 1), i.e. husbandry, environmental effects, and host-pathogen dynamics.

3.1. Husbandry

Table 4 and Fig. 7 show model outputs for an Eastern oyster (*Crassostrea virginica*) farm, using typical growth drivers for the Chesapeake Bay. The farm is 900 m long and 100 m wide, and in ABC it is divided into 5 cultivation sections (Fig. 7), where 0.65 g (live weight) oysters are seeded at day 180 of the year, grown for up to 540 days, and harvested at 70 g (about 8.5 cm in length).⁵ Environmental drivers and culture practice data are taken from Bricker et al. (2018).

Three scenarios are considered, all with an identical set of growth drivers, variable mortality (see Eqs. 3 & 4), and a maximum current speed of 5 cm s⁻¹. For the standard scenario, a low lateral dispersion coefficient ($k_y = 0.018 \text{ m}^2 \text{ s}^{-1}$) is used; each section, or box, is stocked with 1300 kg of oysters, or 2×10^6 animals (200 ind. m⁻²); in between each cultivated section is a 100 m fallowing break. Synthetic results (Table 4) are shown for two further scenarios, which differ as follows from the standard: (i) stocking density is halved to 100 ind. m⁻²; (ii) unchanged stocking, but a fallowing break of 500 m between sections and higher lateral dispersion ($k_y = 0.15 \text{ m}^2 \text{ s}^{-1}$), essentially equivalent to five separate farms along a bay.

The model is configured to automatically harvest oysters as soon as the threshold weight is reached (Harvest When Ready—HWR), and in the standard model the total biomass harvested (Total Physical Product, or TPP) is about 316 metric tons, of which 55% is from the two outer sections of the farm (1 and 5). Food depletion due to oyster filtration severely constrains growth in the inner area, with sections 2, 3, and 4 yielding the remaining 45% of the harvest. The central part of the farm grows only 46.5 t of oysters out of the total farm yield due to food depletion and the first harvestable oysters are only available 40 days after the first harvest in the outer sections.

The return on investment, indicated by the Average Physical Product (APP, i.e. biomass out / biomass in, see Ferreira et al., 2007) reflects food depletion within the farm, with a multiple of about 66 in the outer sections and a sharp decrease to 36 toward the centre of the farm. A more uniform production across a farm of this size could be achieved in four ways: (i) by siting at a location with higher current speeds (we consider a maximum current of 5 cm s⁻¹ to illustrate depletion) and/or more lateral mixing; (ii) by re-locating to an area with higher concentration of food (phytoplankton and detrital organic material); (iii) by reducing stocking density; and/or (iv) by increasing the fallowing break between sections, as long as lateral mixing due to turbulence is sufficient to replenish the food supply to a sufficient degree.

Fig. 7 (upper pane) shows the proportion of harvested, undersized, and dead oysters in each section of the farm: mortality is highest in the central part of the farm, in part because natural mortality is weight-dependent, and therefore smaller animals have a higher chance of dying. Since this scenario implements HWR, i.e. precision aquaculture, undersized animals are in the system for the full culture cycle, rather than being harvested, which increases their overall probability of dying.

⁵ Corresponds to a shell height of 3.3 in.—three inches is a harvest threshold for commercialisation in a number of US states.

The length of time that oysters remain on the farm also affects the clearance rate. In total, the farm filters about $4.5 \times 10^8 \text{ m}^3$ of water over a growth cycle ($3.1 \times 10^8 \text{ m}^3 \text{ y}^{-1}$), but clearance is about 10% higher in the central part of the farm since less oysters are removed through harvest.

The lower pane of Fig. 7 shows food depletion (as chl concentration) and excretion (as dissolved inorganic nitrogen, or DIN) in different farm sections. The two end sections (boxes 1 and 5) are 'noisier', with higher chl when the water flows from upstream, and low chl when the tide turns and the end section downstream receives water that has crossed the whole farm. The central areas of the farm show depletion throughout the culture cycle. An identical pattern can be seen for DIN, reflecting ammonia excretion by the oysters, and the capacity of the outlying water to dilute excess ammonia. The variance in ammonia concentrations is much lower (about 10%) than that observed for chl, where peak ranges over a few tidal cycles can be between 2 and 8 $\mu\text{g L}^{-1}$.

If the stocking density is reduced to 100 ind. m⁻² (Table 4), all the sections of the farm have a harvest of about 80% of the stocked individuals (90% of the biomass) and the variance of chl and DIN is much lower, both among sections and across tidal cycles, and mainly reflects the external conditions driving the model. The lower stocking density shortens the culture cycle—after fourteen months, almost all the oysters have been harvested, and the total yield is just under 283 t, 89% of the harvest with the standard density of 200 ind. m⁻², with half the seed and a far lower environmental footprint—the lower density is clearly a better option with respect to ecological carrying capacity (Inglis et al., 2000; Ferreira et al., 2013b), and leads to a more homogeneous size at harvest, which is also important for the farmer.

3.2. Environmental effects

The environmental effects of high-density shellfish culture have already been discussed (see also lower pane of Fig. 7), the most obvious one being consistent food depletion in the central part of the farm, which makes oyster culture less attractive. If the 100 m fallowing strip is replaced by a 500 m gap between sections, the farm layout can be thought of as 5 different farms, each spaced 0.5 km from the next, such that the total length is 2.5 km. A scenario using moderately high lateral dispersion ($k_y = 12,960 \text{ m}^2 \text{ d}^{-1}$, or $0.15 \text{ m}^2 \text{ s}^{-1}$) was simulated as described above, and the wider gap makes it possible for the inner 'farms' to access food, such that at the standard stocking density the total yield increases to 567 t, 80% higher than the standard harvest.

Gilthead bream (*Sparus aurata*) is one of the key finfish species farmed in Europe, with a reported 2018 production (META, 2020a) of 166 kt.⁶

Fig. 8 shows model results for a 9 ha farm consisting of 5 cultivated sections (boxes) of 1 ha area (100 m × 100 m), each containing one million fish; sections are separated by a 1 ha fallowing gap. Gilthead cages typically contain about $3\text{--}4 \times 10^5$ fish, so each cultivated section can be thought of as having three cages. A maximum current speed of 0.05 m s^{-1} was used, and the simulation considered two-way flow and a semi-diurnal tide. Environmental drivers and culture practice data are taken from Cubillo et al. (In Press).

The results for dissolved oxygen (D.O.) and DIN, as a proxy for ammonia, highlight the difference between an environment with high lateral dispersion ($k_y = 0.2 \text{ m}^2 \text{ s}^{-1}$, upper pane) and no lateral dispersion ($k_y = 0 \text{ m}^2 \text{ s}^{-1}$, lower pane). In a high dispersion scenario, the difference in D.O. among boxes is of the order of 1 mg L⁻¹ and the overall maximum range is about 1.5 mg L⁻¹, whereas with no dispersion the difference doubles and the range can be up to 4–5 mg L⁻¹.

In both scenarios the model shows more tidal variability at the end boxes because these are alternately receiving water from outside the farm

⁶ Eurostat data for 2018 are not yet available for France and Portugal. Based on 2017 data, a further 2.5 kt should be added.

Table 4
ABC outputs for husbandry of Eastern oyster (*Crassostrea virginica*).

Indicator	Section 1	Section 2	Section 3	Section 4	Section 5	Total
Default scenario (200 ind. m ⁻²)						
Seed (kg)	1300	1300	1300	1300	1300	6500
Harvest (TPP, kg)	86,370	48,820	46,552	48,204	86,258	316,204
Average Physical Product (APP)	66.44	37.55	35.81	37.08	66.35	48.65
Non-harvestable (kg)	18,827	47,356	49,267	47,496	19,012	181,957
Mortality (% cycle ⁻¹)	24.3	26.9	27.3	27.2	24.2	
Clearance (10 ⁶ m ³ cycle ⁻¹)	86.23	93.86	93.22	93.53	85.82	452.66
Net N removal (% prod)	0.684	0.759	0.759	0.759	0.681	
Net N removal (% harvest)	0.833	1.494	1.562	1.507	0.832	
Lower density scenario (100 ind. m ⁻²)						
Harvest (TPP, kg)	56,506	56,520	56,121	55,897	57,213	282,257
500 m section breaks, $k_y = 0.15 \text{ m}^2 \text{ s}^{-1}$						
Harvest (TPP, kg)	114,327	112,480	112,383	113,069	115,114	567,373

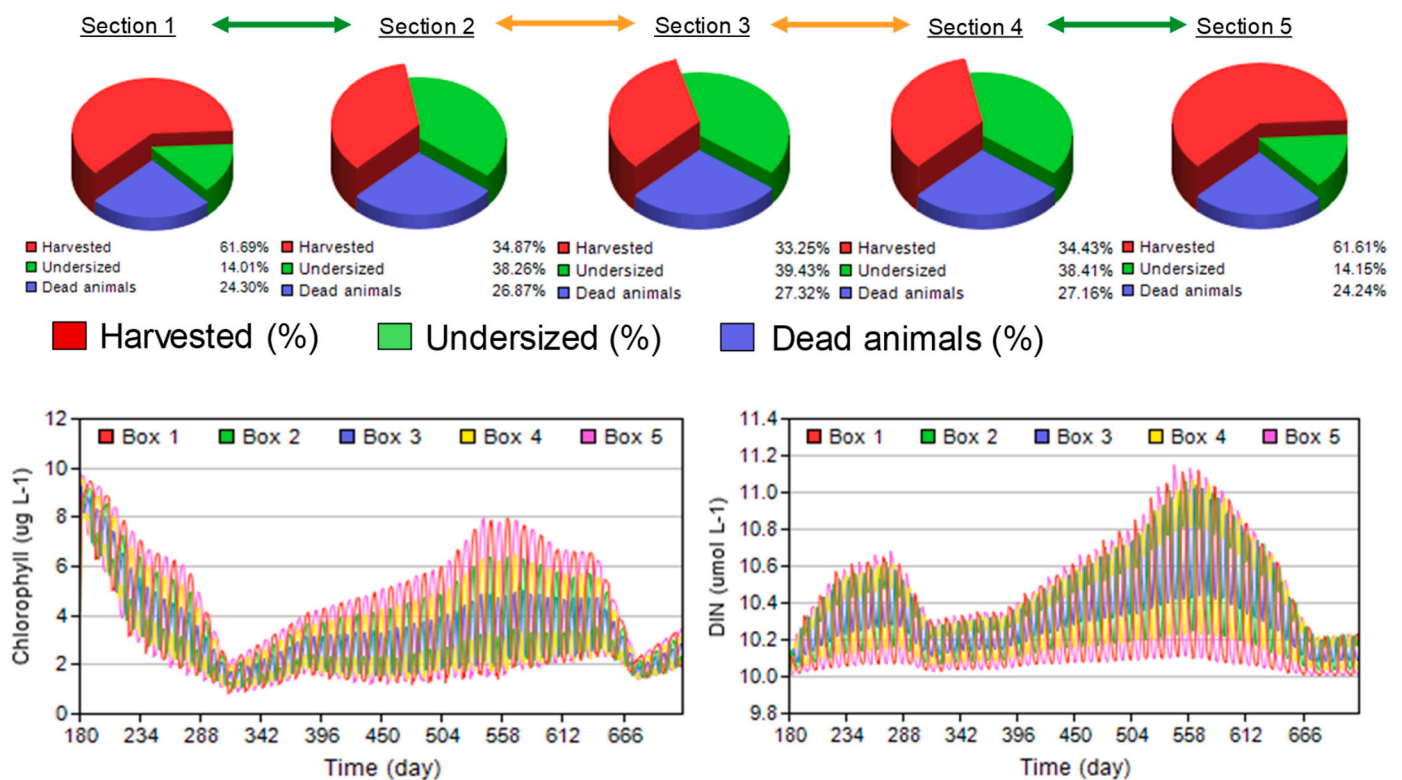


Fig. 7. Proportion of harvested, undersized, and dead biomass in the five cultivated sections of an Eastern oyster (*Crassostrea virginica*) farm (upper pane), and environmental effects of culture (lower pane). Scenario with low dispersion ($k_y = 1555.2 \text{ m}^2 \text{ d}^{-1}$ or $0.018 \text{ m}^2 \text{ s}^{-1}$). Different coloured arrows indicate an increase in food depletion.

and water that has crossed the whole farm, depending on the tidal situation. As a consequence, with no dispersion the water in all but the central part of the farm reaches values of 2–3 mg D.O. L⁻¹, which are at the survival limit for the species, determined to be 2.7 mg L⁻¹, (META, 2020b).

Finfish culture has a much greater effect on both dissolved oxygen and ammonia concentration in the water column than shellfish culture due to the larger size of the animals and the metabolic consequences of this on different water quality parameters. A high stocking density of 200 oysters m⁻², or 2 million animals in an area of 1 ha, is equivalent to a maximum biomass (harvested + non-harvestable, Table 4) of about 105 t in sections 1 and 5. The equivalent fish biomass at typical stocking densities is 324 t, roughly triple that number, but 105 t live weight of oysters corresponds to about 32.7 t fresh tissue weight (Bricker et al., 2018), therefore the real multiple is 10,⁷ i.e. finfish production has a

much greater environmental footprint simply on a metabolic basis, when compared at typical stocking densities per unit area. Furthermore, bivalve shellfish cultivation is organically extractive, and leads to a drawdown of suspended organic material, whereas finfish additionally contribute to the detrital organic pool through uneaten feed.

3.3. Host-pathogen dynamics

The simulation of disease events reported herein considers IHNv in Atlantic salmon, *Vibrio aestuarianus* in Pacific oyster, and a climate change scenario considering OsHV-1 and Pacific oyster.

3.3.1. Atlantic salmon and IHNv

Fig. 9 compares results of an early-stage (30 days after the start of cultivation) and late-stage (405 days after start) IHN virus outbreak. The model is parameterised with data from Tables 3 & 4 and considers weight-dependent natural mortality for all fish and pathogen-related

⁷ Slightly less discounting the weight of the fish skeleton, scales, etc.

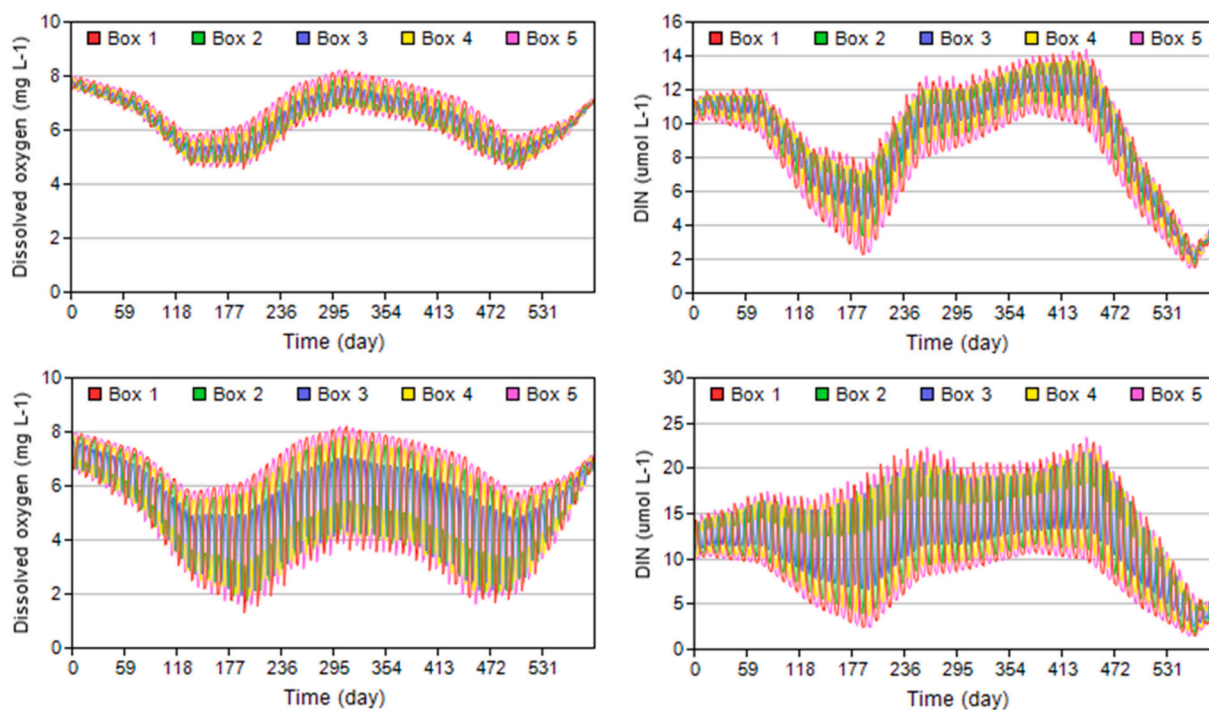


Fig. 8. Dissolved oxygen and DIN (in this case as a proxy for ammonia) in two gilthead bream (*Sparus aurata*) farms. Both farms have an identical layout, stocking density, and other parameters; the only difference is the lateral dispersion coefficient: the upper pane shows a farm with $k_y = 17,280 \text{ m}^2\text{d}^{-1}$ ($0.2 \text{ m}^2\text{s}^{-1}$ i.e. high dispersion) and the lower pane a farm with no lateral mixing ($k_y = 0 \text{ m}^2\text{d}^{-1}$).

mortality for infected fish.

The simulation is set up as previously, with 5 sections, or boxes, of $100 \times 100 \text{ m}^2$ area, separated by a fallowing break (in this case 300 m in length), for a total farm length of 1.7 km. Two-way water flow (maximum speed of 0.05 ms^{-1}) is considered, and a high lateral dispersion coefficient $k_y = 0.2 \text{ m}^2 \text{ s}^{-1}$ helps to disperse the pathogen by promoting turbulent mixing both in cultivated sections and fallowing sections. Each farmed section contains 200,000 salmon, typical for a 50 m diameter polar circle cage in Norway, Scotland, Canada, and Chile; smolt are put in at 80 g, fish are grown for a period of up to 500 days and harvested at 5 kg, using HWR. Environmental drivers and culture practice data follow Cubillo et al. (2016).

The results of an early-stage and late-stage disease event show similar patterns, with a peak in body burden at the start of the infection, showing some lag from between cultivated sections due to water movement across the farm. The upper pane shows the concentration of virus in the water—the pattern for early and late release is similar, but the secondary peak, caused by the tidal reversal, has a higher magnitude for the late release because the infected fish are much larger and shed significantly more virus particles—this is particularly clear for the first section, where the pathogen concentration in the water doubles for the late-stage scenario.

An increase in pathogen concentration in a farm area has potentially serious consequences with respect to interaction with wild fish, a key concern for sustainable aquaculture (Johansen et al., 2011).

The difference between early and late pathogen release can also be seen in the body burden (middle pane), which is an order of magnitude higher for the late release scenario. Since pathogen is only released from a source cage 3 km to the left of section 1 (Table 2), when the tide reverses, section 5 receives uncontaminated water, which explains why sections 5 and 4 have much lower water concentration and body burden, hardly visible in the figure.

This is also reflected in the mortality (lower pane). In both cases, the last two sections (4 & 5) are largely unaffected by pathogen-driven deaths, but the first two sections (1 & 2) are severely impacted, with a loss of up to half the stock.

The results for body burden reflect the internal dynamics of the modelling approach—at present there are no data for comparisons with respect to measured values in tissues. Further comments on scarcity of host-pathogen data are addressed in the final section of this work.

When considered in terms of individuals, the outcomes discussed above appear similar, but when analysed in terms of biomass and from an economic standpoint, the two scenarios are rather different (Table 5).

The harvested biomass in the case of early pathogen release (EPR) and late pathogen release (LPR) are comparable, since roughly the same number of individuals survives the disease event. However, the proportion of dead biomass is much higher for LPR, because the animals were much larger by the time the event occurred. The first section is the most affected, with 397 t of mortalities for LPR, compared to 61 t for EPR.

As a consequence, much more feed was supplied to those animals for LPR prior to the pathogen event: in section 1, about 356 t dry weight of extra feed were used (a cost of 285,000 USD @ 0.8 USD kg^{-1}), which results in a change of Economic Feed Conversion Ratio (FCR_e) of 1.50 for EPR to 2.28 for LPR—since feed corresponds to about 70% of operating costs on a fish farm, this would be a very serious business concern. The biological FCR_b in section 1, which includes mortality (dead biomass) shows a huge difference: FCR_b of 1.74 for EPR to 19.58 for LPR. As the pathogen progresses to other sections, its effect is mitigated due to dilution and die-off, together with the tidal reversal, which brings pathogen-free water to the farm; as a consequence, mortality in section 5 is similar to the background (natural) value, and FCR_e is about 1.5 for both EPR and LPR. From an economic standpoint, the 699 t of extra feed supplied in the LPR scenario correspond to a cost difference of 559,000 USD, or 17 cents kg^{-1} of harvested fish.

This analysis is restricted to the production side, but the costs are considerably higher: they include disposal of dead biomass, disruptive effects on growth and mortality of non-infected fish, potential culling of all the stock, and environmental costs in terms of (i) impacts of waste feed and faeces on bottom sediments; and (ii) oxygen consumption and dissolved nutrient release into the water column due to fish metabolism.

In parts of the world where collection and adequate disposal of

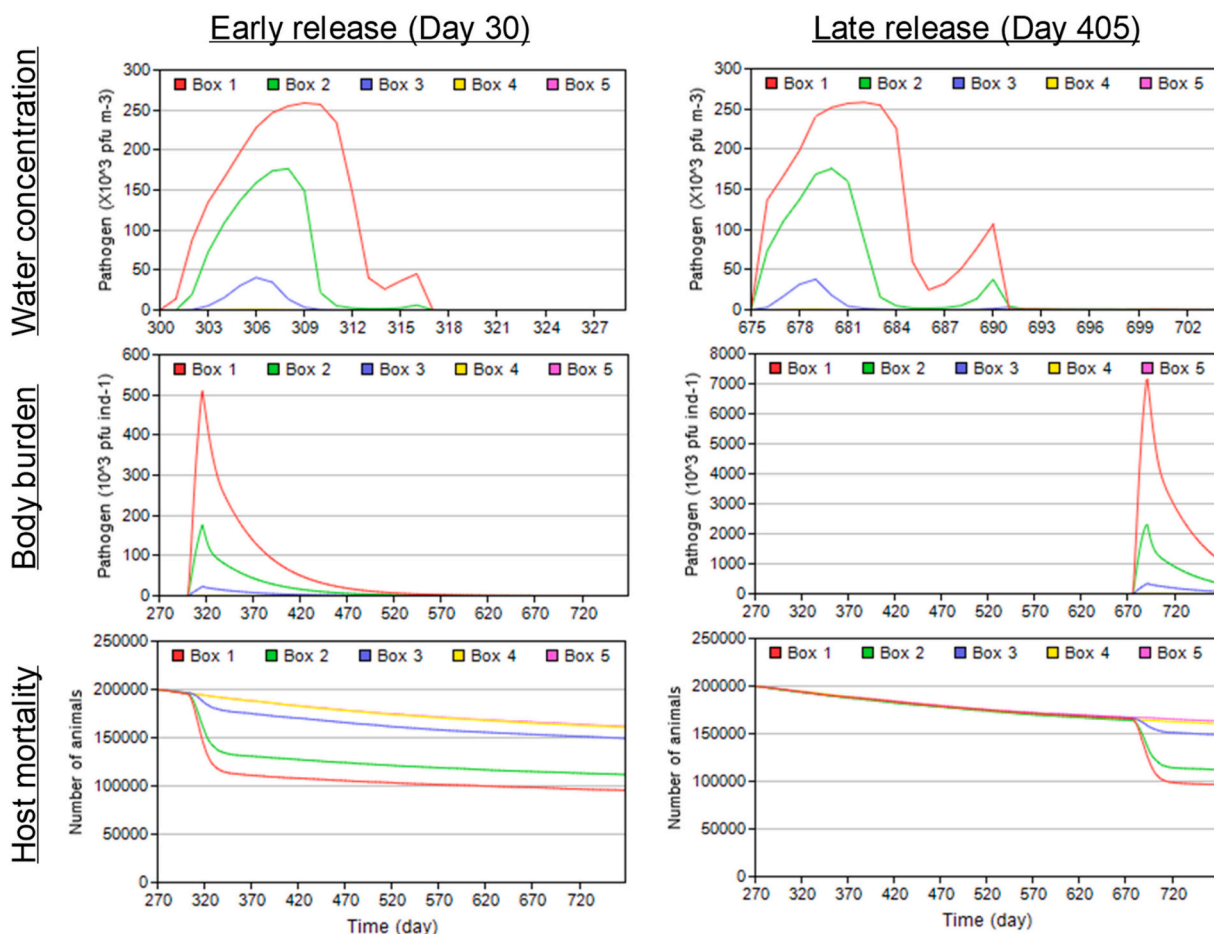


Fig. 9. Pathogen concentration, host body burden, and mortality (as decrease in number of individuals) for early-stage and late-stage infection of Atlantic salmon (*Salmo salar*) with IHNV. Water flow is bidirectional but pathogen is only delivered by an infected source 3 km to the left of section 1.

Table 5

Comparison of selected culture indicators after early-stage (EPR) and late-stage (LPR) pathogen outbreak for IHNV in Atlantic salmon.

Indicator	Scenario	Section 1	Section 2	Section 3	Section 4	Section 5	Farm total
Total harvested biomass (kg)	EPR	463,133	529,959	717,596	767,323	774,114	3,252,125
	LPR	465,455	534,899	713,182	769,799	783,244	3,266,579
Total dead biomass (kg)	EPR	61,133	64,292	67,927	69,791	69,190	332,333
	LPR	396,991	313,966	132,833	75,580	65,747	985,117
Percent dead biomass (%)	EPR	10.03	9.14	7.36	7.06	6.96	–
	LPR	41.74	32.84	13.47	7.60	6.56	–
Feed supplied (kg DW)	EPR	670,583	780,239	1,034,581	1,112,244	1,118,356	4,716,003
	LPR	1,027,004	1,043,067	1,101,073	1,117,214	1,126,909	5,415,267
Feed eaten (kg DW)	EPR	637,054	741,227	982,852	1,056,632	1,062,438	4,480,203
	LPR	975,653	990,914	1,046,019	1,061,354	1,070,564	5,144,504
Economic FCR	EPR	1.50	1.52	1.47	1.48	1.48	–
	LPR	2.28	2.01	1.58	1.48	1.47	–
Biological FCR	EPR	1.74	1.74	1.63	1.63	1.62	–
	LPR	19.58	5.09	1.95	1.65	1.61	–

mortalities are not so well-established, this kind of disease event leads to substantially greater environmental costs—as an example, a mortality event in southern Chile related to a large-scale *Pseudochattonella verruculosa* bloom in 2016 led to offshore dumping of 5000 tons of Atlantic salmon (Díaz et al., 2019).

ABC does not currently include the effect of multi-stressors, such as increased susceptibility to succumbing to infection caused by low dissolved oxygen, but the link between environmental stress and susceptibility to disease is well-established (e.g. Snieszko, 2006). Further research is needed to develop quantitative relationships suitable for incorporating in models—paucity of experimental parameters for host-

pathogen interactions is a current limitation in simulating such multi-stressor effects. Our model does however account for the role of water temperature in terms of host-pathogen overlap—for Atlantic salmon and IHNV, the temperature window is 8–15 °C (Bootland and Leong, 1999), so a pathogen emission can only occur within that range, but the effect of temperature is only on the physiological processes of the host. For bivalve shellfish (discussed below), temperature also conditions clearance rate, thereby affecting the pathogen uptake rate.

3.3.2. Pacific oyster and *Vibrio aestuarianus*

Infection of oysters with various *Vibrio* species is a human health and

food safety problem in many temperate bays and estuaries, due to consumption of infected shellfish (e.g. Froelich and Oliver, 2013). However, *Vibrio aestuarianus* has been shown to cause significant mortality in the host organism itself (Lupo et al., 2019; Table 3), so this host-pathogen pair was selected to illustrate the application of the ABC model to simulate changes in shellfish production and ecosystem services when a disease event occurs.

A five-section (1 ha each) Pacific oyster farm with 100 m following breaks (900 m farm) was used for simulating the host-pathogen dynamics of *Vibrio aestuarianus*, with oyster growth drivers from Carlingford Lough, a transboundary Irish water body (Ferreira et al., 2008). *C. gigas* was stocked at 100 ind. m⁻², cultivated for 850 days—a typical culture cycle in Northern Irish sea loughs—and size-dependent natural mortality was set at a maximum of 20% per year. The validation of individual oyster growth is provided in Cubillo et al. (In Press), together with production and environmental outputs obtained with the FARM model for typical farms.

Fig. 10 shows results for production and ecosystem services (upper pane) and pathogen-related mortality (lower right pane). In ABC, the immune system of infected hosts is simulated to reduce pathogen replication rate as the disease event develops, so that as the initial rate R_i decays to R_f the host body burden is reduced due to shedding. However, the host infectivity is governed in the model by the Hill function (Eq. 10), which uses the pathogen concentration in the water (ID₅₀, Table 3). In farm locations with a significant tidal signal, organisms who survive infection and transition to the exposed and/or to the susceptible state (Fig. 6) can become re-infected and subsequently die due to the persistent high concentration of pathogens in the water column (lower left pane).

The monthly measured water temperature data set contains only one value of 19 °C at Julian day 171, all other values being lower. The emission of *Vibrio aestuarianus* starts at day 160 and lasts for 15 days, and although there is only one day in the whole two-week emission period when the host-pathogen temperature window (19–30 °C, see

Table 3) allows infection, this is enough to cause the disease-related mortality shown in the bottom-right pane of Fig. 10.

In order to compare the results shown with a base case of no disease, the lower threshold temperature at day 171 was changed to 18.99 °C, which will not alter individual growth. Although the disease event is both short-lived and at the early stages of cultivation, it has significant consequences: oyster harvest falls from 194.5 t to 179.3 t, a decrease of 7.8%, and the total net nitrogen removed decreases by 10.2%, partly due to the lower growth, but mainly due to the increased mortality—this is a cost in terms of the provision of regulatory ecosystem services (see review in Ferreira and Bricker, 2019).

Systems where the upper limits of water temperature are extremely close to the minimum required to trigger host-pathogen events are at a tipping point with respect to disease outbreaks; *Vibrio aestuarianus* has been detected in Irish oysters since 2012, whereas in Northern Ireland, the colder waters have so far excluded the pathogen (M. Service, pers. com.), but small interannual fluctuations in water temperature may be enough to trigger quite significant changes in the economics and ecological impacts of shellfish cultivation.

3.3.3. Pacific oyster and oyster herpes virus – climate change

Infection of oysters with the OsHV-1 virus causes significant host mortality in many temperate bays and estuaries—the minimum temperature threshold for outbreaks of herpes in Pacific oysters is 16 °C (Pernet et al., 2015). Given the fact that OsHV-1 has been detected in Europe (e.g. France, Netherlands, UK, Ireland, Spain), the USA, China (Bai et al., 2015), and a number of other countries, the effect of climate change on the oyster industry in risk areas for OsHV-1 is a major management concern.

We used an identical model setup to the *Vibrio* simulations in the previous section, i.e. a 900 m long farm with 100 m following breaks and an identical stocking density. Water temperature was obtained from regionally downscaled climate models simulating end-of-century projections for a worst-case carbon concentration scenario, based on the

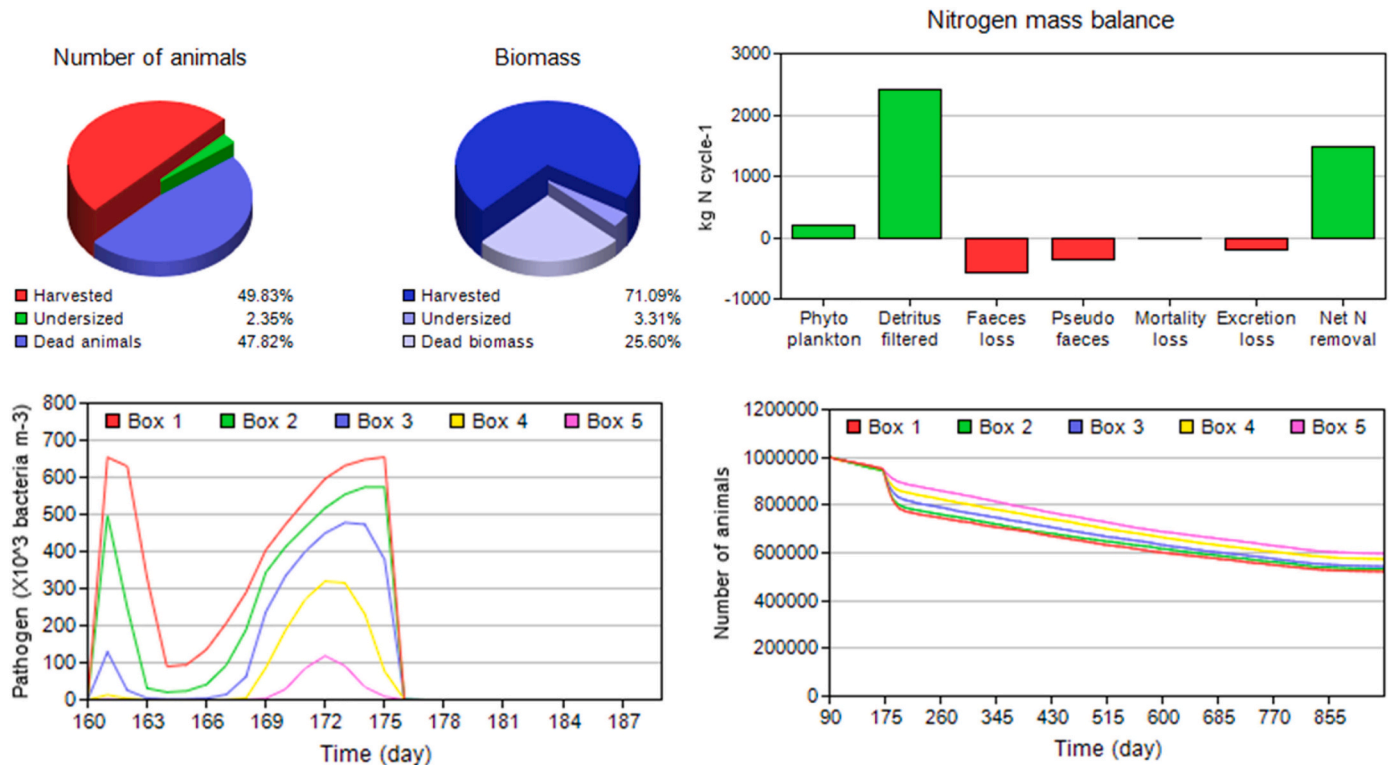


Fig. 10. Production, ecosystem services, and pathogen-derived mortality for Pacific oyster infected with *Vibrio aestuarianus*, using measured data for growth drivers from Carlingford Lough, Ireland/Northern Ireland.

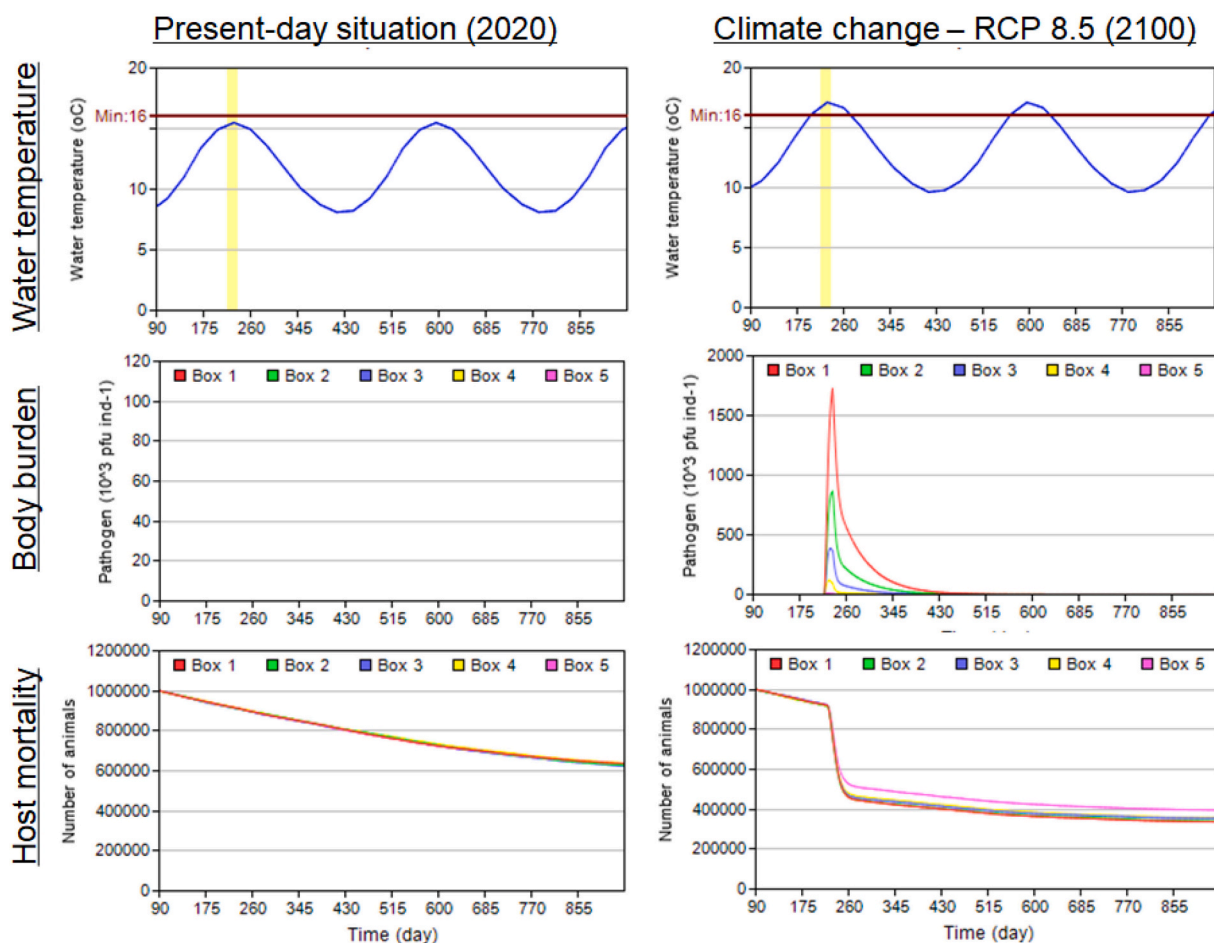


Fig. 11. Water temperature, host body burden, and mortality (as decrease in number of individuals) for modelled current temperature conditions (2020, left pane) and a climate change scenario (RCP 8.5 in 2100) for Pacific oyster (*Crassostrea gigas*) and oyster herpes OsHV-1. Water flow is bidirectional but pathogen is only delivered by an infected source 300 m to the left of section 1. The vertical yellow band in the upper pane represents the pathogen emission window from the source site. (For interpretation of the references to colour in this figure legend, the reader is referred to the pdf version of this article.)

Representative Concentration Pathways (RCP 8.5) provided by the IPCC (van Vuuren et al., 2011). All other growth drivers were identical to the *Vibrio* scenario, and the pathogen outbreak occurred at day 220 and lasted 15 days. The results were compared with ABC outputs using simulated water temperature for 2020 obtained with the climate change model, rather than using measured water temperature data, to ensure consistency across data sets.

Fig. 11 compares the two situations. The present-day (2020) outputs show zero body burden (i.e. no infection) whereas in the climate change

scenario a maximum (mean of all animals) of 1.72×10^6 pfu ind⁻¹ is reached; this is reflected in the mortality curves (lower pane), where the 2020 scenario shows a gradual decline in numbers due to natural mortality, whereas the 2100 scenario shows a catastrophic loss of animals due to pathogen-derived mortality.

The effect of the pathogen is most evident in the first section (Box 1), which is closest to the emission source; by day 266, when the mortality returns to pre-disease rates (< 1000 deaths per day), 5.48×10^5 animals have died in the climate change scenario, compared to 1.07×10^5 (80%

Table 6

Comparison of selected culture indicators for the 2020 baseline and an end-of-century (2100) RCP 8.5 climate change scenario resulting in different host-pathogen overlap windows for Pacific oyster and OsHV-1 (herpes virus) in Carlingford Lough. Water temperature is modelled using a downscaled regional climate model (Van Vuuren et al., 2011; IPCC, 2013). All scenarios use 5×10^6 oysters stocked equally in 5 farm sections, corresponding to a total seeded biomass of 3250 kg.

Indicator	2020 climate model (baseline)	RCP 8.5 Year 2100	Difference due to climate change (%)
Host-pathogen overlap (days)	0	74	
Morts (N° individuals)	1,843,200	3,217,200	+74.5
Dead biomass (t)	75.35	96.33	+27.8
Non-harvestable biomass (t)	73.18	10.86	-85.2
Harvest (t)	142.26	113.67	-20.1
Average Physical Product (APP)	43.77	34.97	-20.1
Water clearance (10 ⁶ m ³)	116.57	69.00	-40.8
Nitrogen removal (t N)	13.84	8.08	-41.6
N removal as percent of harvest	9.7	7.1	-26.8
Individual growth (AquaShell model, g)	80.03	90.44	+13.0

less) in the current scenario. At section (box) 5, furthest from the pathogen source, the corresponding mortalities at day 266 are 4.81×10^5 and 1.08×10^5 , and the reduction is slightly lower (77%).

Table 6 develops this analysis by showing comparative results of production and environmental indicators. Water temperature increase has a positive *direct* effect on Pacific oyster growth; results from the AquaShell individual growth model (Table 6, final row), which drives the IBM model in ABC, show that the end-point weight of a single oyster simulated with the environmental drivers from this scenario increases by 13% at RCP 8.5, to a final weight of 90.44 g. In practice, this means that in ABC, oysters will reach the 70 g weight at which they are harvested earlier with climate change. This is reflected in the mass of non-harvestable animals—those that are below the threshold harvest weight at the end of the culture period—73.18 t in the baseline scenario, compared to 10.86 t (85.2% less) at RCP 8.5. However, the benefit of enhanced growth and earlier harvest is strongly outweighed by the *indirect* effect of climate change on disease mortality, which is 74.5% greater than in the base case.

The consequences for the farmer are of major importance: a 27.8% increase in dead biomass (74.5% increase in dead animals) at RCP 8.5, which would be much worse if this was a late stage outbreak—in the present scenario, oyster weights are in the range of 20–30 g (live weight) across the whole population, but if the OsHV-1 outbreak occurred in the second year of cultivation it would kill oysters in the 50–70 g weight range, with far more damaging effects on harvestable biomass.

Even at the early stage simulated, RCP 8.5 shows a reduction in harvested tonnage of 20.1%, with an identical reduction in APP, i.e. return on investment, and the consequent business liability.

With respect to ecosystem services, the pathogen-driven mortality means that there is a 40.8% reduction in water clearance, a key benefit provided by cultivated filter-feeders (see e.g. Ferreira and Bricker, 2019). As a consequence, less phytoplankton and detrital organic matter is removed, leading to a decrease of 41.6% in net nitrogen removal, and therefore a smaller role of organically extractive aquaculture in top-down control of eutrophication.

Although ABC does not presently simulate synergistic effects of multiple pathogens on a common host, Petton et al. (2015a, 2015b) established that the colonisation of *C. gigas* by a range of vibrios precedes replication of oyster herpes virus OsHV-1, and that whenever Vibrio is not present, a high loading of OsHV-1 is not sufficient to trigger a full-blown infection. The same authors showed that antibiotics reduced mortality rates during an OsHV-1 event, which is further evidence for a bacterial role in herpes outbreaks (Parizadeh et al., 2018).

Even at RCP 8.5 in 2100, the outputs of the downscaled climate models used in this OsHV-1 scenario do not reach the critical temperature of 19 °C, above which Vibrio kills Pacific oysters. However, climate models have a relatively coarse grid, and is quite probable that bays, estuaries, and fjords will show more extreme ranges than open marine systems—this raises concerns for future outbreaks of both Vibrio and herpes as a consequence of climate change.⁸

4. Conclusions

The work presented herein is the first approach that allows a combined analysis of three key components of carrying capacity (Fig. 1), viz.: husbandry, environmental effects, and pathogen interaction. Both positive and negative environmental effects can be considered, such as reduction of eutrophication symptoms (sensu Bricker et al., 2003) due to top-down control by filter-feeders and hypoxia in open water finfish farms if the cages are placed too close or sited in areas with insufficient mixing.

⁸ These concerns partly explain why there has been a substantial increase in oyster farming in Ireland by French producers in recent years due to the reduced risk of crop loss due to oyster herpes virus in colder water.

To our knowledge, ABC is the first pathogen model that simulates pathogen uptake as a function of water concentration, integrates pathogen, production, and biogeochemical modelling, and allows the simulation of pathogen body burden within the host, rather than infection through contact. Nevertheless, it is important to emphasise that the model works only for pathogens with direct life cycles, not for those with complex life cycles such as sea lice (e.g. Sandvik et al., 2020). This is partly because ABC, like FARM, is a local-scale model, and thus cannot address the multiple life-cycle stages of organisms such as *Lepophtheirus* sp. and *Caligulus* sp.

A great deal of work has been devoted to modelling the production of cultivated aquatic organisms, and the environmental factors that increase or constrain it, with the objective of enhancing sustainable aquaculture production. However, without accounting for the potential effects of a pathogen outbreak on mortality, such models are necessary but not sufficient as a tool to address production carrying capacity (sensu Inglis et al., 2000). We illustrated this by means of a number of modelling outcomes where pathogen outbreaks played a clear role in the potential commercial viability of a farm.

We have shown how the ABC framework can provide decision support for both managers and industry by analysing a range of factors that condition carrying capacity and siting of farms, including issues related to overstocking (food depletion), proximity of culture structures (hypoxia), and effects of water renewal on these issues. In addition, the analysis of host-pathogen interactions highlighted the use of ABC to examine the consequences of early stage versus late stage pathogen infection in terms of impacts e.g. on FCR and APP. The economic and ecological risks of cultivation in a changing climate, as environmental variables reach host-pathogen overlap thresholds, also provided industry stakeholders with concrete examples of use in business planning and risk assessment over the next decades.

ABC is a standalone platform that falls into the category of screening models (Ferreira et al., 2012b), and is designed from a technical standpoint specifically for industry and managers, with respect to ease of use and practical application.

The combination of deterministic and stochastic modelling used in ABC is an appropriate way to address growth, environmental effects, and disease, but this work laid bare the paucity of epidemiological data required to effectively apply such combined approaches, and therefore the key research need for quantitative data on host-pathogen pairs. The complexity of such research is by no means underestimated by the authors, but it is important to highlight that the current limitations in advancing this combined approach lie much more with the stochastic host-pathogen component than with a need for further parameterisation of the deterministic simulation of physiological processes.

Since pathogen issues often occur at a system scale; the ABC farm-scale approach does not consider interactions at a bay or estuary level. Nevertheless, distance transmissions can be accounted for by assuming a low-level underlying background pathogen level, which would lead to a low probability of triggering an epidemic within a farm. Once infection occurs in a farm site, these distant infections are of little relevance as the level of infection in the farm site will be what drives the process. Transport of animals and relaying can be important infection routes, which are easily captured in the existing framework simply by changing the number of susceptible and infected animals in the population at the time of the new stock being introduced to a site.

Interactions between production and environment with respect to growth drivers, as well as risks such as organic loading to the sediment and consequences thereof, are presently at a level of understanding which is acceptable for decision-making; however, relationships between environmental conditions and successful pathogen outbreaks are less well understood in quantitative terms, and this limits the ability to model such synergistic effects and their consequences both for industry and ecosystem equilibrium.

These challenges should be seen as opportunities to further develop models of this kind, based on a unified approach to carrying capacity

assessment, which are able to address physical, production, ecological, and to some degree social aspects of this complex and divisive issue. Tools of this nature, and their quantitative outputs, will help inform the discussion on aquaculture outcomes and help optimise the societal benefits of growing good fish in terms of nutrition, taste, animal welfare, environmental sustainability, and local employment.

Declaration of Competing Interest

The authors whose names are listed immediately below certify that they have NO affiliations with or involvement in any organization or entity with any financial interest (such as honoraria; educational grants; participation in speakers' bureaus; membership, employment, consultancies, stock ownership, or other equity interest; and expert testimony or patent-licensing arrangements), or non-financial interest (such as personal or professional relationships, affiliations, knowledge or beliefs) in the subject matter or materials discussed in this manuscript.

Acknowledgements

The authors acknowledge various sources of direct or indirect funding, including EU Horizon 2020 CERES (G.A. 678193) and GAIN (G. A. 773330) projects, EU INTERREG (IVA5025) SWELL project, NOAA EPA REServ grant MOA-2011-025/8258, and NOAA NCCOS Discretionary Science Budget, & Sea Grant Aquaculture Extension and Technology Transfer. In addition, we wish to thank S.B. Bricker (NOAA), M. Service & H. Moore (AFBI), J. Johansen (GIFAS), and C. Lupo (IFREMER) for helpful discussions during the development of this work. We are grateful to three reviewers for comments on an earlier draft of the text.

References

- Ferreira, J.G., Saurel, C., Ferreira, J.M., 2012a. Cultivation of gilthead bream in monoculture and integrated multi-trophic aquaculture. Analysis of production and environmental effects by means of the FARM model. *Aquaculture* 358–359, 23–34. <https://doi.org/10.1016/j.aquaculture.2012.06.015>.
- Ferreira, J.G., Aguilar-Manjarrez, J., Bacher, C., Black, K., Dong, S.L., Grant, J., Hofmann, E., Kapetsky, J., Leung, P.S., Pastres, R., Strand, Ø., Zhu, C.B., 2012b. Progressing aquaculture through virtual technology and decision making tools for novel management. In: FAO/NACA, 2012. Farming the Waters for People and Food, Subasinghe, R.P., Arthur, J.R., Bartley, D.M., De Silva, S.S., Halwart, M., Sorgeloos, P. (Eds.), Proceedings of the Global Conference on Aquaculture 2010, Phuket, Thailand. 22–25 September 2010. FAO, Rome and NACA, Bangkok, pp. 643–704.
- Ferreira, J.G., Grant, J., Verner-Jeffreys, D., Taylor, N., 2013a. Carrying capacity for aquaculture, modeling frameworks for determination of. In: Meyers, Robert A. (Ed.), Encyclopedia of Sustainability Science and Technology. Springer, pp. 1–32. ISBN: 978-0387894690.
- Ferreira, J., Ramos, L., Costa-Pierce, B.A., 2013b. Key drivers and issues surrounding carrying capacity and site selection, with emphasis on environmental components. In: Ross, L.G., Telfer, T.C., Falconer, L., Soto, D., Aguilar-Manjarrez, J. (Eds.), Site selection and carrying capacities for inland and coastal aquaculture, FAO/Institute of Aquaculture, University of Stirling, Expert Workshop, 6–8 December 2010. Stirling, the United Kingdom of Great Britain and Northern Ireland FAO Fisheries and Aquaculture Proceedings 21. FAO, Rome, pp. 47–86 (282 pp.).
- OIE, 2019. Aquatic Animal Health Code. OIE, Paris, France.
- Alaliyat, S., Yndestad, H., Davidsen, P.L., 2019. An agent-based approach for predicting patterns of pathogen transmission between aquaculture sites in the Norwegian fjords. *Aquaculture* 505, 98–111.
- Anderson, R.M., Jackson, A.C., May, R.M., Smith, A.M., 1981. Population dynamics of fox rabies in Europe. *Nature* 289, 765–771.
- Atalah, J., Sanchez-Jerez, P., 2020. Global assessment of ecological risks associated with farmed fish escapes. *Global Ecology and Conservation* 21. <https://doi.org/10.1016/j.gecco.2019.e00842>.
- Bai, C., Wang, C., Xia, J., Sun, H., Zhang, S., Huang, J., 2015. Emerging and endemic types of Ostreid herpesvirus 1 were detected in bivalves in China. *J. Invertebr. Pathol.* 124, 98–106.
- Bidegain, E.N., Powell, J.M., Klinck, E.E., Hofmann, T., Ben-Horin, D., Bushek, S.E., Ford, D.M., Munroe, X. Guo, 2017. Modeling the transmission of *Perkinsus marinus* in the Eastern oyster *Crassostrea virginica*. *Fish. Res.* 186, 82–93. <https://doi.org/10.1016/j.fishres.2016.08.006>.
- Bootland, L.M., Leong, J.C., 1999. Infectious hematopoietic necrosis virus. editors. In: PTK, Woo, Bruno, D.W. (Eds.), Fish diseases and disorders. CAB International, New York, pp. 57–121.
- Adams, T., Black, K., MacIntyre, C., MacIntyre, I., Dean, R., 2012. Connectivity modelling and network analysis of sealice infection in Loch Fyne, west coast of Scotland. *Aquacult. Environ. Interact.* 3, 51–63.
- Bricker, S.B., Ferreira, J.G., Simas, T., 2003. An integrated methodology for assessment of estuarine trophic status. *Ecol. Model.* 169 (1), 39–60.
- Bricker, S.B., Ferreira, J.G., Zhu, C.B., Rose, J.M., Galimany, E., Wikfors, G.H., Saurel, C., Landeck Miller, R., Wands, J., Trowbridge, P., Grizzle, R.E., Wellman, K., Rheault, R., Steinberg, J., Jacob, A.P., Davenport, E.D., Ayyavazian, S., Chintala, M., Tedesco, M.A., 2018. The role of shellfish aquaculture in reduction of eutrophication in an urban estuary. *Environ. Sci. Technol.* 52 (1), 173–183.
- Brigolin, D., Maschio, G.D., Rampazzo, F., Giani, M., Pastres, R., 2009. An individual-based population dynamic model for estimating biomass yield and nutrient fluxes through an off-shore mussel (*Mytilus galloprovincialis*) farm. *Estuar. Coast. Shelf Sci.* 82, 365–376. <https://doi.org/10.1016/j.ecss.2009.01.029>.
- Cantrell, D., Filgueira, R., Revie, C.W., Rees, E.E., Vanderstichel, R., Guo, M., Foreman, M.G.G., Wan, D., Grant, J., 2020. The relevance of larval biology on spatiotemporal patterns of pathogen connectivity among open-marine salmon farms. *Can. J. Fish. Aquat. Sci.* 77 (3), 505–519.
- Cressey, D., 2009. Future fish- news feature. *Nature* 458, 398–400. <https://doi.org/10.1038/458398a>.
- Cubillo, A.M., Ferreira, J.G., Robinson, S.M.C., Pearce, C.M., Corner, R.A., Johansen, J., 2016. Role of deposit feeders in integrated multi-trophic aquaculture - a model analysis. *Aquaculture* 453, 54–66.
- Cubillo, A.M.C., Ferreira, J.G., Pearce, C.M., Marshall, R., Cheney, D., Hudson, B., 2018. Ecosystem services of geoduck farming in South Puget Sound, USA: a modeling analysis. *Aquac. Int.* <https://doi.org/10.1007/s10499-018-0291-x>.
- Cubillo, A.M., Ferreira, J.G., Lencart Silva, J., Taylor, N.G.H., Kennerley, A., Guilder, J., Kay, S., Kamermans, P. Projected effects of climate change on productivity of European aquaculture. *Aquac. Int.* (In Press).
- Díaz, P.A., Álvarez, G., Varela, D., Pérez-Santos, I., Díaz, M., Molinet, C., Seguel, M., Aguilera-Belmonte, A., Guzmán, L., Uribe, E., Rengel, J., Hernández, C., Segura, C., Figueroa, R.I., 2019. Impacts of harmful algal blooms on the aquaculture industry: Chile as a case study. Perspectives in Phycology 6 (1–2), 39–50. <https://doi.org/10.1127/pip/2019/0081>.
- European Commission, 2018. Facts and Figures on the Common Fisheries Policy. European Commission, 52 pp.
- Eurostat, 2019. Data sourced through Eurostat webservices. available at. <https://longline.co.uk/meta>.
- Evans, O., Hick, P., Dhand, N., Whittington, R.J., 2015. Transmission of Ostreid herpesvirus-1 in *Crassostrea gigas* by cohabitation: effects of food and number of infected donor oysters. *Aquac. Environ. Interact.* 7, 281–295. <https://doi.org/10.3354/AEI00160>.
- FAO (Food and Agriculture Organization of the United Nations), 2008. Fishery and Aquaculture Statistics. FAO yearbook, Rome.
- FAO (Food and Agriculture Organization of the United Nations), 2014. Fishery and Aquaculture Statistics. FAO yearbook, Rome.
- FAO (Food and Agriculture Organization of the United Nations), 2016. The State of World Fisheries and Aquaculture (SOFIA). FAO, Rome, 204 pp.
- FAO (Food and Agriculture Organization of the United Nations), 2020. The State of World Fisheries and Aquaculture (SOFIA). FAO, Rome, 224 pp.
- Ferreira, J.G., 1995. EcoWin - an object-oriented ecological model for aquatic ecosystems. *Ecol. Model.* 79, 21–34.
- Ferreira, J.G., Bricker, S.B., 2019. Assessment of Nutrient Trading Services from Bivalve Farming. In: Smaal, Aad C., Ferreira, Joao G., Grant, Jon, Petersen, Jens K., Strand, Øivind (Eds.), Goods and Services of Marine Bivalves, pp. 551–584. Editors.
- Ferreira, J.G., Hawkins, A.J.S., Monteiro, P., Moore, H., Service, M., Pascoe, P.L., Ramos, L., Sequeira, A., 2008. Integrated assessment of ecosystem-scale carrying capacity in shellfish growing areas. *Aquaculture* 275, 138–151.
- Ferreira, J.G., Saurel, C., Lencart e Silva, J.D., Nunes, J.P., Vazquez, F., 2014a. Modelling of interactions between inshore and offshore aquaculture. *Aquaculture* 426–427, 154–164.
- Ferreira, J.G., Hawkins, A.J.S., Bricker, S.B., 2007. Management of productivity, environmental effects and profitability of shellfish aquaculture - the FARM aquaculture resource management (FARM) model. *Aquaculture* 264, 160–174.
- Ferreira, J.G., Falconer, L., Kittiwanih, J., Ross, L., Saurel, C., Wellman, K., Zhu, C.B., Suvanachai, P., 2014b. Analysis of production and environmental effects of Nile tilapia and white shrimp culture in Thailand. *Aquaculture*. <https://doi.org/10.1016/j.aquaculture.2014.08.042>.
- Filgueira, R., Guyonnet, T., Comeau, L.A., Grant, J., 2014. A fully-spatial ecosystem-DEB model of oyster (*Crassostrea virginica*) carrying capacity in the Richibucto estuary, eastern Canada. *J. Mar. Syst.* 136, 42–54.
- Flores-Kossacka, C., Montero, R., Köllner, B., Maisey, K., 2020. Chilean aquaculture and the new challenges: pathogens, immune response, vaccination and fish diversification. *Fish & Shellfish Immunology* 98, 52–67.
- Føre, M., Alver, M., Alfredeen, J.A., Marafioti, G., Senneset, G., Birkevold, J., Willumsen, F.V., Lange, G., Espmarke, Å., Terjesen, B.F., 2016. Modelling growth performance and feeding behaviour of Atlantic salmon (*Salmo salar* L.) in commercial-size aquaculture net pens: model details and validation through full-scale experiments. *Aquaculture* 464, 268–278.
- Froelich, B., Oliver, J.D., 2013. The interactions of *Vibrio vulnificus* and the oyster *Crassostrea virginica*. *Microb. Ecol.* 65 (4) <https://doi.org/10.1007/s00248-012-0162-3>.
- Gangnery, A., Chabirand, J.M., Lagarde, F., Le Gall, P., Oheix, J., Bacher, C., Buestel, D., 2003. Growth model of the Pacific oyster, *Crassostrea gigas*, cultured in Thau lagoon (Mediterranean, France). *Aquaculture* 215, 267–290.

- Gangnery, A., Bacher, C., Buestel, D., 2004. Application of a population dynamics model to the Mediterranean mussel, *Mytilus galloprovincialis*, reared in Thau lagoon (France). *Aquaculture* 229, 289–313. [https://doi.org/10.1016/S0044-8486\(03\)00360-0](https://doi.org/10.1016/S0044-8486(03)00360-0).
- Garver, K.A., Mahony, A.A.M., Stucchi, D., Richard, J., Van Woensel, C., Foreman, M., 2013. Estimation of parameters influencing waterborne transmission of infectious hematopoietic necrosis virus (IHNV) in Atlantic salmon (*Salmo salar*). *PLoS One* 8. <https://doi.org/10.1371/journal.pone.0082296>.
- Grøttum, J.A., Sigholt, T., 1998. A model for oxygen consumption of Atlantic salmon (*Salmo salar*) based on measurements of individual fish in a tunnel respirometer. *Aquac. Eng.* 17 (4), 241–251. [https://doi.org/10.1016/S0144-8609\(98\)00012-0](https://doi.org/10.1016/S0144-8609(98)00012-0).
- Hernández, J.M., Gasca-Leyva, Eucario, León, Carmelo J., Vergara, J.M., 2003. A growth model for gilthead seabream (*Sparus aurata*). *Ecol. Model.* 165, 265–283.
- Hoffmann, E.E., Powell, E.N., Klinck, J.M., Saunders, G., 1995. Modelling diseased oyster populations I. modelling *Perkinsus marinus* infections in oysters. *J. Shellfish Res.* 14 (1), 121–151.
- META—Maritime and Environmental Thresholds for Aquaculture, 2020a. Processed Eurostat data on European aquaculture obtained from. <http://longline.co.uk/meta>.
- META—Maritime and Environmental Thresholds for Aquaculture, 2020b. Thresholds for dissolved oxygen for gilthead bream obtained from. <http://longline.co.uk/meta>.
- Fisheries and Oceans Canada, 2020. Annual statistics on the volume and value of aquaculture production in Canada. <https://www.dfo-mpo.gc.ca/stats/aqua/aqua18-eng.htm>.
- Japan Center for Economic Research (JCER), 2018. Medium-Term Forecast of Asian Economies: 2018–2030. JCER. <https://www.jcer.or.jp/english/emerging-cities-sin-king-cities-in-asia-by-2030>.
- Inglis, G.J., Hayden, B.J., Ross, A.H., 2000. An overview of factors affecting the carrying capacity of coastal embayments for mussel culture. In: NIWA Client Report CHC00/69, Christchurch, New Zealand.
- IPCC, 2013. Climate Change 2013: The Physical Science Basis. In: Stocker, T.F., Qin, D., Plattner, G.-K., Tignor, M., Allen, S.K., Boschung, J., Midgley, P.M. (Eds.), Contribution of Working Group I to the Fifth Assessment Report of the Intergovernmental Panel on Climate Change. Cambridge University Press, Cambridge, United Kingdom and New York, NY, USA, 1535 pp.
- Johansen, L.-H., Jensen, I., Mikkelsen, H., Bjørn, P.-A., Jansen, P.A., Bergh, Ø., 2011. Disease interaction and pathogen exchange between wild and farmed fish populations with special reference to Norway. *Aquaculture* 315 (3–4), 167–186.
- Jones, A.E., Munro, L.A., Green, D.M., Morgan, K.L., Murray, A.G., Norman, R., Ryder, D., Salama, N.K.G., Taylor, N.G.H., Thrush, M.A., 2019. The contact structure of Great Britain's salmon and trout aquaculture industry. *Epidemics* 28, 100342.
- Kermack, W.O., McKendrick, A.G., 1927. Contributions to the mathematical theory of epidemics—I. *Proceedings of the Royal Society* 115A, 700–721.
- Lopes, A.S., Ferreira, J.G., Vale, C., Johansen, J., 2017. The mass balance of production and consumption: supporting policy-makers for aquatic food security. *Estuar. Coast. Shelf Sci.* 188, 212–223.
- Lupo, C., Travers, M.A., Tourbiez, D., Barthélémy, C.F., Beaunée, G., Ezanno, P., 2019. Modeling the transmission of *Vibrio aestuarianus* in Pacific oysters using experimental infection data. *Front. Vet. Sci.* 6, 142. <https://doi.org/10.3389/fvets.2019.00142>.
- McKenney, D.G., Kurath, G., Wargo, A.R., 2016. Characterization of infectious dose and lethal dose of two strains of infectious hematopoietic necrosis virus (IHNV). *Virus Res.* 214, 80–89.
- McKindsey, C.W., Thetmeyer, H., Landry, T., Silvert, W., 2006. Review of recent carrying capacity models for bivalve culture and recommendations for research and management. *Aquaculture* 261 (2), 451–462.
- Murray, A.G., 2009. Using simple models to review the application and implications of different approaches used to simulate transmission of pathogens among aquatic animals. *Prev. Vet. Med.* 88, 167–177.
- Murray, G., D'Anna, L., 2015. Seeing shellfish from the seashore: the importance of values and place in perceptions of aquaculture and marine social-ecological system interactions. *Mar. Policy* 62, 125–133.
- Nobre, A.M., Ferreira, J.G., Nunes, J.P., Yan, X., Bricker, S., Corner, R., Groom, S., Gu, H., Hawkins, A., Hutson, R., Lan, D., Lencart e Silva, J.D., Pascoe, P., Telfer, T., Zhang, X., Zhu, M., 2010. Assessment of coastal management options by means of multilayered ecosystem models. *Estuar. Coast. Shelf Sci.* 87, 43–62.
- Nobre, A.M., Valente, L.M.P., Conceição, L., Severino, R., Lupatsch, I., 2019. A bioenergetic and protein flux model to simulate fish growth in commercial farms: application to the gilthead seabream. *Aquac. Eng.* 84, 12–22.
- Nunes, J.P., Ferreira, J.G., Bricker, S.B., O'Loan, B., Dabrowski, T., Dallaghan, B., Hawkins, A.J.S., O'Connor, B., O'Carroll, T., 2011. Towards an ecosystem approach to aquaculture: assessment of sustainable shellfish cultivation at different scales of space, time and complexity. *Aquaculture* 315, 369–383.
- Parizadeh, L., Tourbiez, D., Garcia, C., Haffner, P., Degremont, L., Le Roux, F., Travers, M.A., 2018. Ecologically realistic model of infection for exploring the host damage caused by *Vibrio aestuarianus*. *Environ. Microbiol.* 20, 4343–4355. <https://doi.org/10.1111/1462-2920.14350>.
- Paul-Pont, I., Evans, O., Dhand, N.K., Whittington, R.J., 2015. Experimental infections of Pacific oyster *Crassostrea gigas* using the Australian ostreid herpesvirus-1 (OSHV-1) μ var strain. *Dis. Aquat. Org.* 113, 137–147. <https://doi.org/10.3354/dao02826>.
- Pernet, F., Tamayo, D., Petton, B., 2015. Influence of low temperatures on the survival of the Pacific oyster (*Crassostrea gigas*) infected with ostreid herpes virus type 1. *Aquaculture* 445, 57–62. <https://doi.org/10.1016/j.aquaculture.2015.04.010>.
- Petton, B., Boudry, P., Alumno-Bruscia, M., Pernet, F., 2015a. Factors influencing disease-induced mortality of Pacific oysters *Crassostrea gigas*. *Aquac. Environ. Interact.* 6, 205–222. <https://doi.org/10.3354/aei00125>.
- Petton, B., Bruto, M., James, A., Labreuche, Y., Alumno-Bruscia, M., Le Roux, F., 2015b. *Crassostrea gigas* mortality in France: the usual suspect, a herpes virus, may not be the killer in this polymicrobial opportunistic disease. *Front. Microbiol.* 6, 686.
- Press, W.H., Teukolsky, S.A., Vetterling, W.T., Flannery, B.P., 2002. Numerical recipes in C++. In: The Art of Scientific Computing, 2nd ed. Cambridge University Press. 1002 pp.
- Ren, J.S., Ross, A.H., 2001. A dynamic energy budget model of the Pacific oyster *Crassostrea gigas*. *Ecol. Model.* 142, 105–120.
- Salama, N.K.G., Murray, A.G., 2011. Farm size as a factor in hydrodynamic transmission of pathogens in aquaculture fish production. *Aquaculture Environment Interactions* 2 (1), 61–74.
- Salama, N.K.G., Rabe, B., 2013. Developing models for investigating the environmental transmission of disease causing agents within open-cage salmon aquaculture. *Aquaculture Environment Interactions* 4 (2), 91–115.
- Sandvik, A.D., Johnsen, I.A., Mykssvoll, M.S., Sævik, P.N., Skogen, M.D., 2020. Prediction of the salmon lice infestation pressure in a Norwegian fjord. *ICES J. Mar. Sci.* 77 (2), 746–756. <https://doi.org/10.1093/icesjms/fsz256>.
- Saurel, C., Ferreira, J.G., Cheney, D., Suhrbier, A., Dewey, B., Davis, J., Cordell, J., 2014. Ecosystem goods and services from Manila clam culture in Puget Sound: a modelling analysis. *Aquaculture Environment Interactions* 5, 255–270.
- Schikorski, D., Faury, N., Pepin, J.F., et al., 2011a. Experimental ostreid herpesvirus 1 infection of the Pacific oyster *Crassostrea gigas*: kinetics of virus DNA detection by q-PCR in seawater and in oyster samples. *Virus Res.* 155, 28–34. <https://doi.org/10.1016/j.virusres.2010.07.031>.
- Schikorski, D., Renault, T., Saulnier, D., et al., 2011b. Experimental infection of Pacific oyster *Crassostrea gigas* spat by ostreid herpesvirus 1: demonstration of oyster spat susceptibility. *Vet. Res.* 42, 1–13. <https://doi.org/10.1186/1297-9716-42-27>.
- Shafer, C.S., Inglis, G.J., Martin, V., 2010. Examining Residents' proximity, recreational use, and perceptions regarding proposed aquaculture development. *Coast. Manag.* 38 (5), 559–574. <https://doi.org/10.1080/08920753.2010.511700>.
- Silvert, W., 1993. Object-oriented ecosystem modelling. *Ecol. Model.* 68, 91–118.
- Smaal, A.C., Prins, T.C., Dankers, N., Ball, B., 1998. Minimum requirements for modelling bivalve carrying capacity. *Aquat. Ecol.* 31, 423–428.
- Sniezko, S.F., 2006. The effects of environmental stress on outbreaks of infectious diseases in fishes. *J. Fish Biol.* 6 (2), 197–208. <https://doi.org/10.1111/j.1095-8649.1974.tb04537.x>.
- Soto, D., Aguilar-Manjarrez, J., Brugère, C., Angel, D., Bailey, C., Black, K., Edwards, P., Costa-Pierce, B., Chopin, T., Deudero, S., Freeman, S., Hambrey, J., Hishamunda, N., Knowler, D., Silvert, W., Marba, N., Mathe, S., Norambuena, R., Simard, F., Tett, P., Troell, M., Wainberg, A., 2008. Applying an ecosystem-based approach to aquaculture: principles, scales and some management measures. In: Soto, D., Aguilar-Manjarrez, J., Hishamunda, N. (Eds.), Building an Ecosystem Approach to Aquaculture, FAO/Universitat de les illes Balears Expert Workshop. Palma de Mallorca, FAO, Rome, pp. 15–35 (FAO Fisheries and Aquaculture Proceedings 14), 7–11 May 2007.
- Stavrakidis-Zachou, O., Papandroulakis, N., Lika, K., 2019. A DEB model for European sea bass (*Dicentrarchus labrax*): parameterisation and application in aquaculture. *J. Sea Research* 143, 262–271.
- Stigebrandt, A., Aure, J., Ervik, A., Hansen, P.K., 2004. Regulating the local environmental impact of intensive marine fish farming III. A model for estimation of the holding capacity in the Modelling-Ongrowing fish farm-Monitoring system. *Aquaculture* 234, 239–261.
- Taylor, N.G.H., Norman, R.A., Way, K., Peeler, E.J., 2011. Modelling the koi herpesvirus (KHV) epidemic highlights the importance of active surveillance within a national control policy. *J. Appl. Ecol.* 48, 348–355.
- Tiller, R., Gentry, R., Richards, R., 2013. Stakeholder driven future scenarios as an element of interdisciplinary management tools: the case of future offshore aquaculture development and the potential effects on fishermen in Santa Barbara, California. *Ocean Coast. Manag.* 73, 127–135.
- Travers, M.A., Tourbiez, D., Parizadeh, L., et al., 2017. Several strains, one disease: experimental investigation of *Vibrio aestuarianus* infection parameters in the Pacific oyster, *Crassostrea gigas*. *Vet. Res.* 48, 1–8. <https://doi.org/10.1186/s13567-017-0438-1>.
- Van der Veer, H.W., Cardoso, J.F.M.F., Van der Meer, J., 2006. The estimation of DEB parameters for various Northeast Atlantic bivalve species. *J. Sea Res.* 56, 107–124.
- Van Vuuren, D.P., Edmonds, J., Kainuma, M., Riahi, K., Thomson, A., Hibbard, K., Hurtt, G.C., Kram, T., Krey, V., Lamarque, J.F., Masui, T., Meinshausen, M., Nakicenovic, N., Smith, S.J., Rose, S.K., 2011. The representative concentration pathways: an overview. *Clim. Chang.* 109, 5. <https://doi.org/10.1007/s10584-011-0148-z>.
- Váradi, L., Lane, A., Harache, Y., Gyalog, G., Békefi, E., Lengyel, P., 2011. Regional Review on Status and Trends in Aquaculture Development in Europe – 2010. FAO Fisheries and Aquaculture Circular No. 1061/1. Rome, FAO. 257 pp.